Observations of Chromospheric Anemone Jets with Hinode/SOT and Hida Ca II Spectroheliogram

Satoshi Morita, Kazunari Shibata, Satoru Ueno, Kiyoshi Ichimoto, Reizaburo Kitai, and Ken-ichi Otsuji Kwasan and Hida Observatories, Kyoto University,
Kurabashira, Kamitakara, Takayama, Gifu 506-1314
morita@kwasan.kyoto-u.ac.jp

(Received 2009 July 4; accepted 2009 December 14)

Abstract

We present the first simultaneous observations of chromospheric "anemone" jets in solar active regions with Hinode/SOT Call H broadband filetergram and Call K spetroheliogram on the Domeless Solar Telescope (DST) at Hida Observatory. During the coordinated observation, 9 chromospheric anemone jets were simultaneously observed with the two instruments. These observations revealed three important features, i.e.: (1) the jets are generated in the lower chromosphere, i.e. these cannot be seen in CaII K₃, (2) the length and lifetime of the jets are 0.4-5 Mm and 40-320 sec, (3) the apparent velocity of the jets with Hinode/SOT are 3-24 km/s, while Ca II K₃ component at the jets show blueshifts (in 5 events) in the range of 2-6 km/s. The chromospheric anemone jets are associated with mixed polarity regions which are either small emerging flux regions or moving magnetic features. It is found that the CaII K line often show red or blue asymmetry in K₂/K₁ component: the footpoint of the jets associated with emerging flux regions often show redshift (2-16 km/s), while the one with moving magnetic features show blueshift ($\sim 5 \text{ km/s}$). Detailed analysis of magnetic evolution of the jet foaming regions revealed that the reconnection rate (or canceling rate) of the total magnetic flux at the footpoint of the jets are of order of 10^{16} Mx/s, and the resulting magnetic energy release rate $(1.1-10)\times10^{24}$ erg/s, with the total energy release $(1-13) \times 10^{26}$ erg for the duration of the magnetic cancellations, ~130s. These are comparable to the estimated total energy, $\sim 10^{26}$ erg, in a single chromospheric anemone jet. In addition to Hida/DST Ca II-K Spectroheliogram and Hinode/SOT Ca II H broadband filetergram, we also used Hinode/SOT magnetogram as well as Hida H α filtergram. An observation-based physical model of the jet is presented. The relation between chromospheric anemone jets and Ellerman bombs is discussed.

Key words: Sun: actvity — Sun: chromosphere — Sun: magnetic fields

1. Introduction

The Solar Optical Telescope (SOT) (Tsuneta et al. Suematsu et al. 2008a) onboard (Kosugi et al. 2007) has discovered ubiquitous tiny jets in the active region chromosphere, called chromospheric anemone jets, with CaII H broadband filter observations (Shibata et al. 2007). These jets are typically 3-7 arcsec (2-5 Mm) long, and 0.2-0.4 arcsec (0.15–0.3 Mm) wide, and their apparent velocity is 10–20 km/s. Their morphology shows the inverted Y shape, which is quite similar to the shape of coronal X-ray anemone jet discovered by Yohkoh (Shibata et al. 1992, 1994, Shimojo et al. 1996). Detailed observational analysis using magnetogram (Shimojo, Shibata, & Harvey 1998) and magnetohydrodynamic numerical simulations (Yokoyama & Shibata 1995, 1996) of the X-ray anemone jet showed that the anemone shape is foamed as a result of magnetic reconnection, so it can be an indirect observational evidence of the magnetic reconnection in the solar corona. These findings have been recently confirmed and extended to even smaller X-ray jets with the X-Ray Telescope (XRT) onboard Hinode (Cirtain et al. 2007, Shimojo et al. 2007, Savcheva et al. 2007).

The discovery of ubiquitous tiny chromospheric anemone jets suggests that these jets may be generated by the magnetic reconnection similar to that occurring in the corona. Recently, Shibata et al. (2007) reported in their preliminary observations that some of the footpoint of the jets correspond to the mixed magnetic polarities, suggesting reconnection in the photosphere or chromosphere. The total energy involved in a single chromospheric anemone jet was estimated to be 10^{25} erg, which is comparable to the energy of nanoflares proposed ideal by Parker (1988). Hence it may be interesting to study the relation between these ubiquitous jets and the coronal heating, although at present the number of these jets are too small to explain the coronal heating (Shibata et al. 2007). It should be stressed that there are even more smaller jets or jet-like features in the chromosphere whose footpoints are not well resolved so by definition they cannot be identified as the chromospheric anemone jet. (Note that a chromospheric anemone jet has a bright footpoint that has an anemone shape, or inverted Y shape structure.)

There are number of unanswered questions concerning the chromospheric anemone jet, e.g., What is the true velocity (Doppler velocity) of these jets? Are mixed polarities universal at the footpoint of these jets? What is the relation to other chromospheric jets, such as surges (e.g., Rust 1968, Roy 1973, Kubota et al. 1974, Schmieder et al. 1995, Canfield et al. 1996, Liu & Kurokawa 2004, Brooks et al. 2007), H α jets (e.g., Chae et al. 1999), EUV jets (e.g., Brueckner & Bartoe 1983, Alexander & Fletcher 1999), and spicules (e.g., Beckers 1972, Nishikawa 1988, Suematsu et al. 1995, Sterling 2000, De Pontieu et al. 2007, Suematsu et al. 2008b)? The footpoint of chromospheric anemone jets reminds us of similar tiny brightening features, called Ellerman bombs (e.g., Ellerman 1917, Roy & Leparskas 1973, Kurokawa et al. 1982, Kitai 1983, Nindos & Zirin 1998, Qiu, et al. 2000, Geolgoulis et al. 2002, Pariat et al. 2004, Fang et al. 2006, Pariat et al. 2007, Matsumoto et al. 2008a, 2008b, Watanabe et al. 2008). So the question arises whether the footpoints of these jets correspond to the Ellerman bombs.

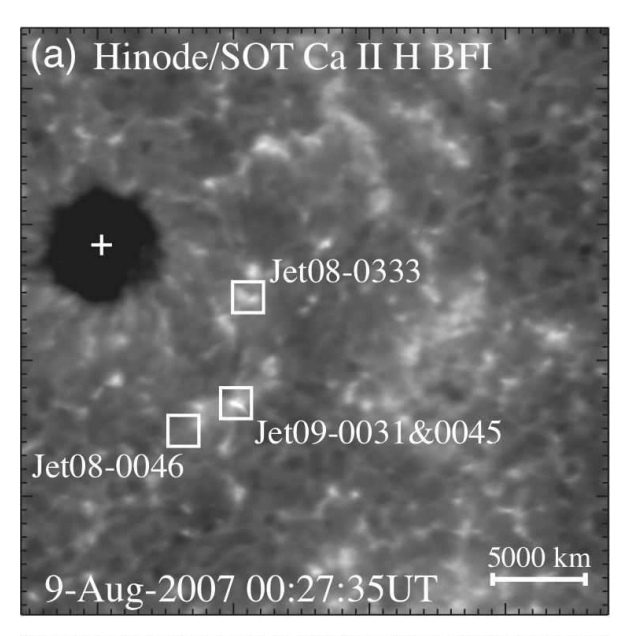
In this paper, we report the first simultaneous observations of the chromospheric anemone jets with SOT/Hinode CaII H broadband filter and CaII K spectroheliogram on the Domeless Solar Telescope (DST) at Hida Observatory (Nakai & Hattori 1985). Since the Hinode/CaII H filter is a broadband filter, it is not possible to derive velocity and other information such as occurrence height of the jets. Using the spectroheliogram on DST, we first derived the true Doppler velocity and height information of the chromospheric anemone jet. In this paper, we have made comprehensive analysis of the chromospheric anemone jets, also using SOT/Hinode magnetogram data as well as Hida H α filtergram, to develop an observation-based physical model of the jet.

The paper is organized in the following manner: In section 2, we present observational method for both Hinode and Hida observations, and in section 3, we describe observational results for typical three examples of the chromospheric anemone jets in very detail. Finally, we discuss the energy release rate and the physical model of the jets.

2. Observation

In order to study evolution and dynamics of the chromospheric anemone jets and the related phenomena, we performed coordinated observations of the active region, using the SOT/Hinode Broadband Filter Imager (BFI) of Filtergraph (FG) and the 60 cm Domeless Solar Telescope of the Hida Observatory, Kyoto University. These observations were performed under the Hinode Observation Plan 12 (HOP12). The most important purpose of HOP12 was to get the simultaneous observations of dynamic phenomena such as jets with the Hinode Ca II H BFI as well as DST/Hida Ca II K spectroheliograph.

The target region in this study was NOAA AR 10966 and its surrounding area. The time of the central meridian passing through the active region was around 11:00 UT on August 9, 2007. For the present study, we used the data set covering the period from 23:00 UT on August 6 to 01:00 UT on August 10, 2007. The total observing time of the data set was approximately 25 hours. The angle between the line-of-sight and the vector normal to the horizontal plane at the target region ranged from 36 to 13



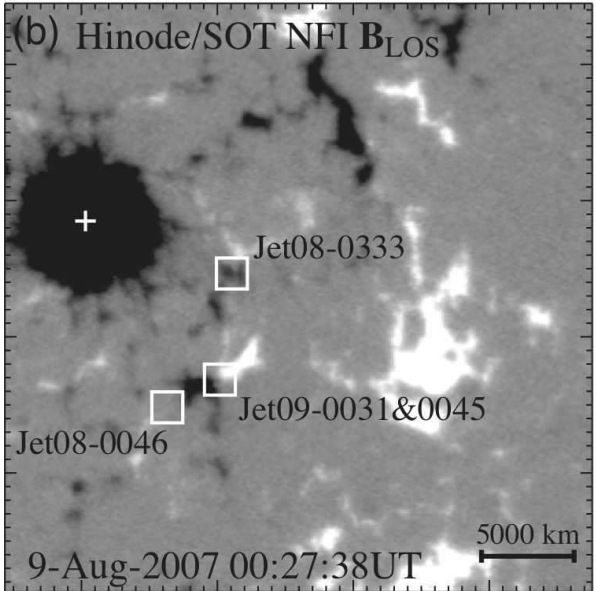


Fig. 1. The locations of four typical chromospheric anemone jets and their surrounding area (moat region of NOAA AR 10966) observed with (a) the CaII H broadband filter equipped by the SOT/Hinode, and with (b) the FeI 6302Å narrowband filter equipped by the SOT (Stokes V/I magnetogram): The time of the images are chosen for "Jet09-0031". The boxes indicates the locations of the four typical jets, which we introduce in section 3.2. Each jet location is measured on the local frame centered on the sunspot, and the location is transferred to the observed frame with the time of the images. Top is north and left is east. FOV of each image is 43."2×43."2.

degrees (between 0.81 and 0.97 in $\mu = \cos \theta$, see Table 1), so it was an "on disk" observation.

2.1. Hinode SOT observation

The observations with the SOT/Hinode BFI were performed in 2×2 summing mode (0".109/pixel), covering an area of $56"\times112"$ (before 06:00 UT on August 8, 2007) or

an area of $83'' \times 83''$ (rest of the period) in the data set. The time cadence of the Ca II H BFI images was 15 seconds till 11:00 UT on August 7, 2007 and 40 seconds for the rest of the period. The normal calibration processes were performed on the BFI images. Thereafter the images were coaligned with each other using the sunspot.

In order to investigate the magnetic environment surrounding the jets as well as dynamical changes in the photospheric magnetic field at the "footpoints of the jets", we examined the Stokes data as well. We also used the SOT Narrowband Filter Imager (NFI) of FG observations with the Stokes IQUV shutterless mode (cf. Ichimoto et al. 2008) for the spectral band of Fe I 6302 Å absorption line in the HOP12. The cadence of NFI Stokes observations were the same as that for the BFI Ca II H images. The time difference between each NFI and BFI observations was 6 seconds. The shutterless mode Stokes IQUV data were available from 12:00 UT on August 7, 2007. The data covered an area of $51'' \times 164''$ in 2×2 summing mode (0''.16/pixel). The passband of the narrowband filter is 84mÅ (FWHM), that was positioned at -120mÅ of the Fe i 6302.5 Å line. Dark subtraction, the correction of bad pixels, and cosmic-ray removal were applied. The polarization calibration was applied to the NFI data following Ichimoto et al. (2008). Depending on the spectral band, scaling corrections to BFI data and alignments within the NFI images and the NFI and BFI images were applied. A weak field approximation is adopted for filtergrams (cf. Landi degl'Innocenti & Landolfi 2004) to interpret the NFI Stokes IQUV data for the construction of magnetograms.

Figure 1a shows the Ca II H broadband filter snapshot image of the AR 10966 at 00:27:35 UT on August 9, 2007, near the disk center. A typical chromospheric anemone jet ("Jet09-0031") is visible in the south-west region of the sunspot. The length and the width of the jet are 1000 km and 200 km, respectively. The velocity of the jet is estimated to be 9.7 km/s (see Table 1). These parameter values are similar to those of the chromospheric anemone jet, reported by Shibata et al. (2007) observed near the limb.

2.2. Hida DST observation

The observations for the CaII K spectroheliograph in this study were obtained with the vertical spectrograph of the 60 cm Domeless Solar Telescope of the Hida Observatory, Kyoto University. The wavelength coverage was about 16 Å around the core of Ca II K line (3933.68) Å). The wavelength sampling was 0.021 Å per pixel. The spectrograph slit had a width of 50 μ m (0".32 on the sun), and scanning step and range were 0".40 and 98", respectively. The slit length corresponded to about 144" on the sun, with the pixel resolution along the slit of 0''.24 per pixel. Dark subtractions and flat-field corrections were applied to each of the spectrograms in the sequence. The wavelengths of two photospheric lines (Fe I blend 3932.64 Å and Fe i 3935.32 Å), each averaged along the entire length of the slit, were used as the wavelength references for each exposure. Intensity corrections to the spectroheliograms were applied by fitting the averaged quiet region spectrum with the Sacramento Peak Atlas (Beckers, Bridges, & Gilliam 1976) so that the intensity unit of a spectroheliogram becomes ${\rm erg/s/cm^2/\mathring{A}}$. Thereafter the observed intensity is converted into the flux emitted at the solar surface with assuming isotropic radiation from jets and their surrounding area. The distance between the sun and the Earth $(1.52\times10^8~{\rm km})$ and the solar radius $(6.96\times10^5~{\rm km})$ are used for this conversion.

Figure 2 shows a Ca II K line profile of a chromospheric anemone jet ("Jet09-0031") taken with the DST/Hida vertical spectroheliograph. The broken curve in Fig. 2a shows the SOT/Hinode Ca II H filter profile, which is shifted to the Ca II K line. Figures 2b–2h show spectroheliograms made in various wavelengths shown in Fig. 2a.

DST/Hida also equips a 0.25 Å passband $H\alpha$ Lyot filter, and takes images at five wavelength positions ($H\alpha$ center and its wing at ± 0.5 Å and ± 0.8 Å) without disturbing the Ca II K spectroheliograph observation. We use these $H\alpha$ Lyot filter images for extracting additional spectral information in the chromosphere, and for understanding the magnetic connectivities in the chromosphere in the region around jets. The details of $H\alpha$ observations are discussed in the Appendix.

3. Results

3.1. Overview of the observed region

The active region AR 10966 had an umbra with negative magnetic polarity, while the southwestern half of the moat region was dominated by positive magnetic polarity (see Fig. 1b). A boundary of the magnetic polarities in the moat region and the sunspot was located in the west side of the umbra, and this is a favorable site for the emerging flux in the active region. A strong activity of emerging flux started in this part of the active region around 22 UT on August 7, 2007, then a new umbra was formed in the north side of the original umbra around 12 UT on August 8, 2007 (see Fig. 2).

During the coordinated observation, 9 chromospheric anemone jets were observed simultaneously with Hinode Ca II H broadband filter and DST/Hida Ca II K spectroheliograms. Table 1 shows the basic properties of 9 jets. In the following section, evolution and dynamics of four typical jets out of these 9 jets are discussed. All of the four jets occurred with magnetic flux cancellations at the photosphere. The opposite polarity magnetic elements around the cancellation sites were converged by the extensions of EFRs or Moat flow.

3.2. Case study

3.2.1. Jets associated with emerging flux (Aug. 9 0031 and 0045)

It is found that the location of the jets lies near the boundary between the positive and negative magnetic polarities or the polarity inversion line (PIL in Fig. 4f). A series of jets (five or more) has occurred on the same polarity inversion line during a period of around 45 minutes,

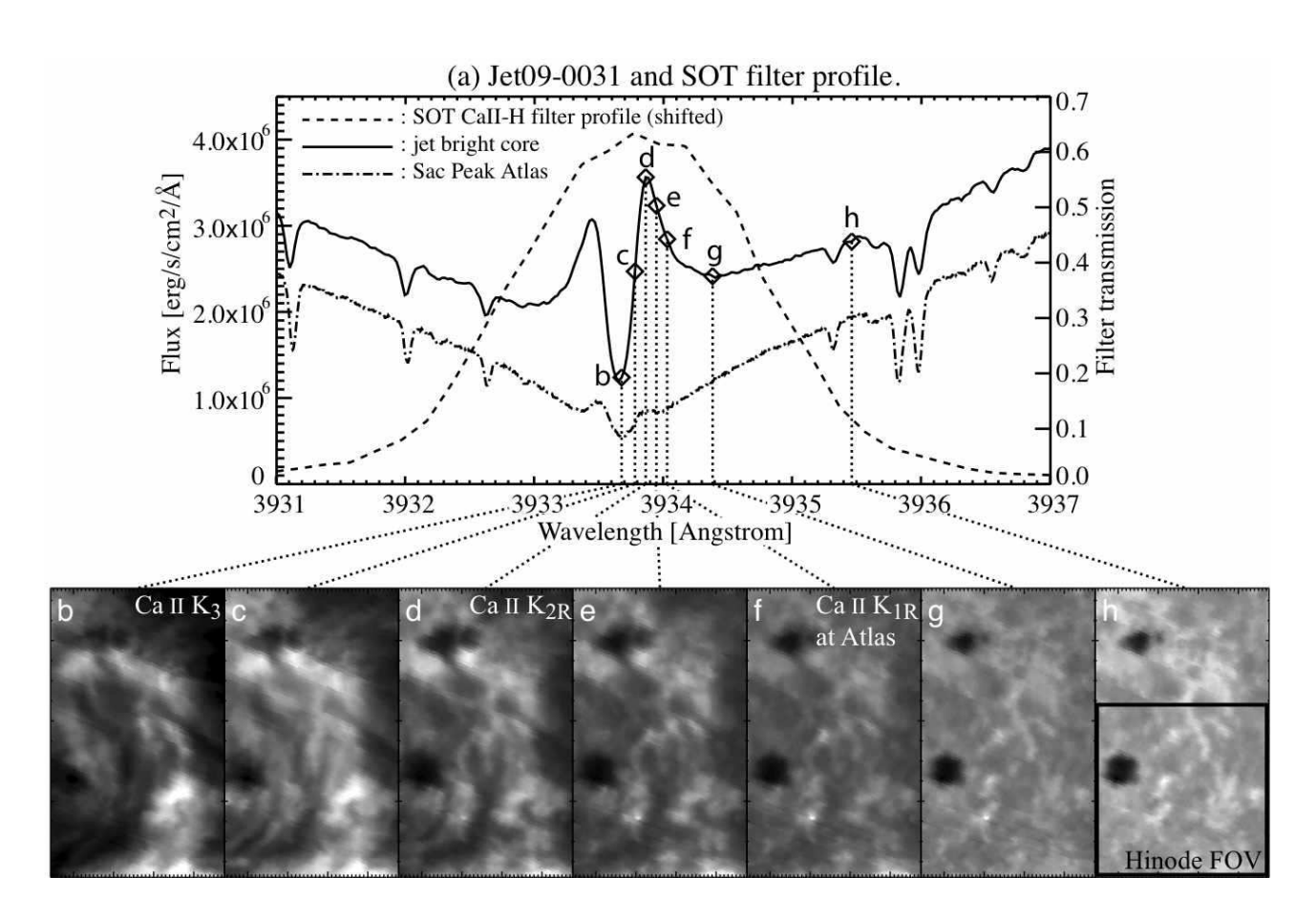


Fig. 2. (a) A typical Ca II K line profile of a chromospheric anemone jet's bright core taken with the DST/Hida vertical spectrometer at 00:27:45 UT around the jet bright core in Figure 1: The solid curve in (a) represents the Ca II K line profile of the jet bright core. The broken curve in (a) shows the SOT/Hinode Ca II H filter profile, which is shifted to the Ca II K line. The dash-dotted curve in (a) shows the Ca II K line profile from the Sac Peak Atlas. Frames (b)–(h) show the spectroheliograms at the wavelengths indicated by diamonds in (a). Top is north and left is east. Each image in (b)–(h) has the same FOV of $0.72'\times1.2'$. The smaller FOV in (h) represent the SOT/Hinode FOV of Fig. 1.

Table 1. Basic Data of SOT Ca II Jets around NOAA AR10966.

Event	SOT Ca II H	μ^*	Life	Max I/	Area	Max	V_{\perp}	V_{LOS}^{\ddagger}	Ca II K ₁ /K ₂
Name	Peak time		$_{ m time}$	quiet I	size^\dagger	length			asymmetry
	(UT)		(sec)		$(\mathrm{Mm^2})$	(Mm)	(km/s)	(km/s)	
Jet07-0301	2007 Aug 07 03:01	0.82	180	1.79	1.23	1.16	6.5	-5.7	red
Jet08-0046	Aug 08 00:46	0.92	320	1.95	1.85	1.49	4.6	-0.8	blue
Jet08-0319	03:19	0.93	40	1.79	1.99	2.81	2.8	0.0	red
Jet08-0333	03:33	0.93	170	1.53	1.85	2.71	13.6	-1.9	red
Jet08-0430	04:30	0.93	200	1.61	0.65	4.81	24.1	2.7	not obvious
Jet09-0031	Aug 09 00:31	0.97	270	2.02	0.49	0.86	9.7	-2.2	red
Jet09-0045	00:45	0.97	240	2.28	0.73	0.45	5.1	-2.3	red
Jet09-2350	23:50	0.97	180	1.85	0.37	0.56	3.1	-3.4	red
Jet 10-0011	Aug 10 00:11	0.97	90	2.06	0.33	1.02	11.2	0.0	not obvious

^{*} $\mu = \cos\theta$, where θ is the heliocentric angle.

 $^{^{\}dagger}$ area size of bright features at SOT Ca II H intensity peak time.

 $^{^{\}ddagger}$ by Doppler shift of the CaII K₃ absorption line. "blue shift" is negative. Estimated error is ± 1.6 km/s.

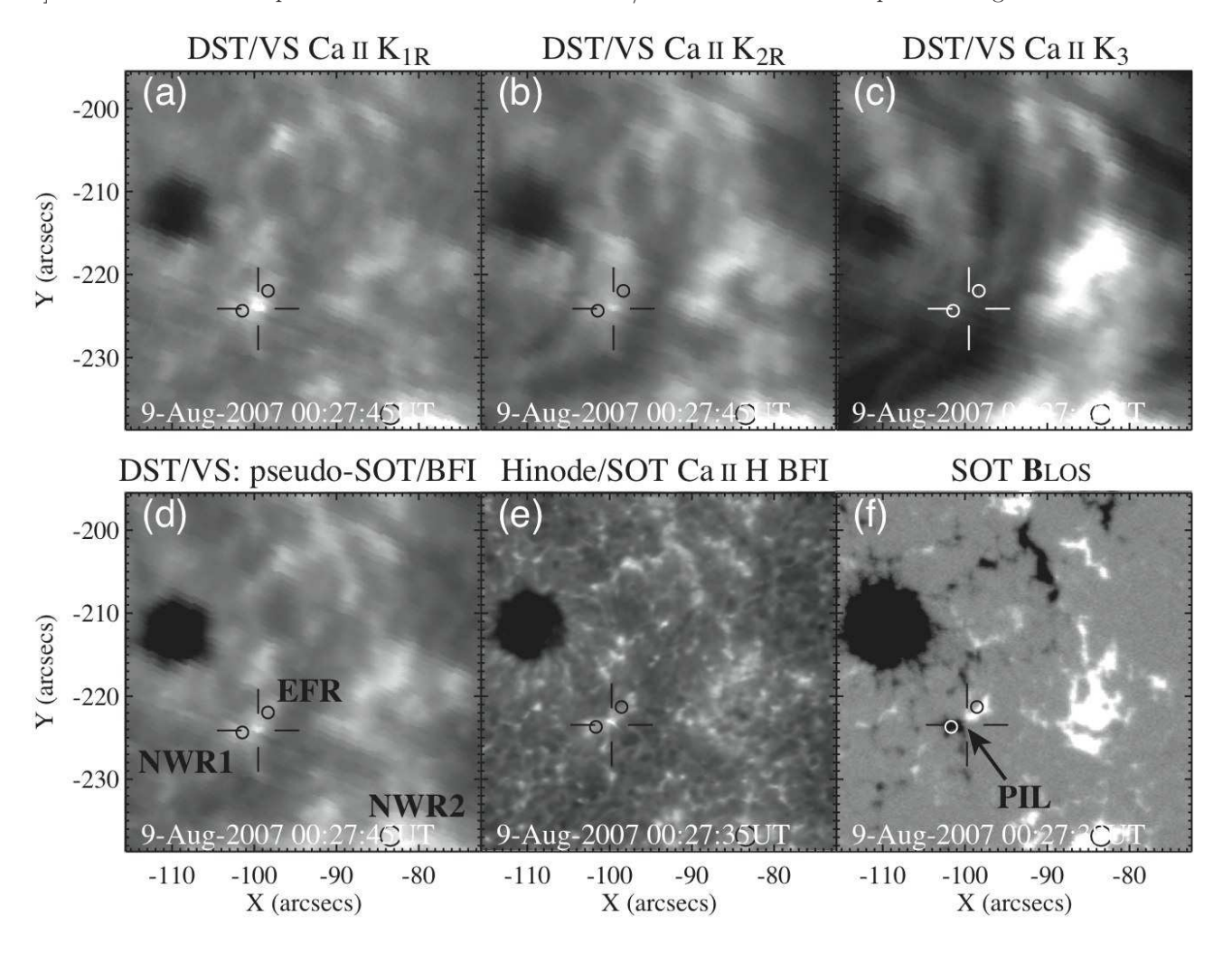


Fig. 4. The DST/Hida Ca II K spectroheliograms of (a) Ca II K_{1R} , (b) Ca II K_{2R} , (c) Ca II K_{3} , and (d) a pseudo Ca II K broadband image made of the DST Ca II K spectroheliograms and the SOT Ca II H broadband filter profile (cf. Fig. 2a), and the corresponding SOT images of (e) BFI Ca II H, and (f) NFI photospheric magnetogram: Top is north and left is west. Each image has the same FOV of Fig. 1. The cross-hairs indicates the jet core brightening location. The circles indicate the locations of an EFR and network regions (EFR, NWR1, and NWR2), in which the average spectra are shown in Fig. 5. White and black in frame (f) represent positive and negative magnetic polarities (color is saturated at ± 300 Gauss). The arrow indicates the polarity inversion line (PIL) where the jet occurred.

centered in around 00:45 UT on August 9, 2007. Figure 3 shows the time variation of the BFI Ca II H intensity at the locations on the same polarity inversion line (see PIL in Fig. 4f). Every single intensity peak in the light curve represents a "single" jet event.

The first large peak indicated by oblique hatching in Fig. 3 represents the "Jet09-0031" (see Table 1), which was seen in Fig. 1 and 2. The spectroheliograms in CaII K_{1R} , K_{2R} , and K_{3} of this jet event at 00:27:45UT (3 minutes before the CaII H intensity peak; see Fig. 3) along with its surrounding area are shown in Figures 4a–c. Fig. 4d shows the pseudo-Hinode CaII H image for this region, and Fig. 4e depicts the SOT BFI CaII H image from Fig. 1 for comparison. Although the spatial resolution is very different (0."2 for Hinode and 1" for DST/Hida with seeing condition), overall morphology is still similar. Comparison between the four CaII spectroheliograms and Hinode CaII H image reveals that the Hinode CaII jet is

formed below the middle chromosphere, since the jet cannot be seen in K₃ image. Fig. 4f shows the SOT/Hinode NFI photospheric magnetogram of the same field of view. It is found the polarity inversion line was formed by the continuous collision between a positive polarity source of a newly emerging dipole (shown by black circle in Fig. 4f; EFR), and an isolated negative source in the moat region (open circle in Fig. 4f; NWR1).

Figure 5 shows the CaII K spectra of the "Jet09-0031" at the time of the spectroheliograms in Fig. 4. The solid curve in Fig. 5a represents the averaged spectrum at the jet bright core. In order to demonstrate the emission increased by the jet, we compared the CaII K emission spectrum from the jet bright core with the spectra from the nearest CaII K network regions of this jet (dotted and broken curves). The spectrum from the jet bright core shows a characteristic intensity increase from the spectra of the nearest network regions, widely ($\sim 4.8 \text{Å}$) around K₁. We

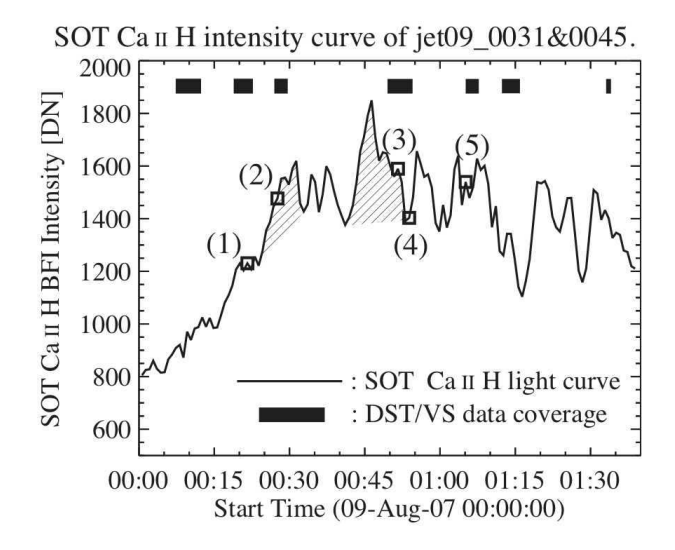
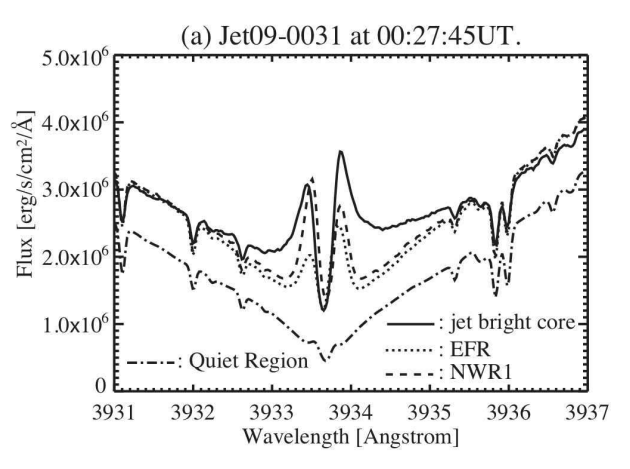
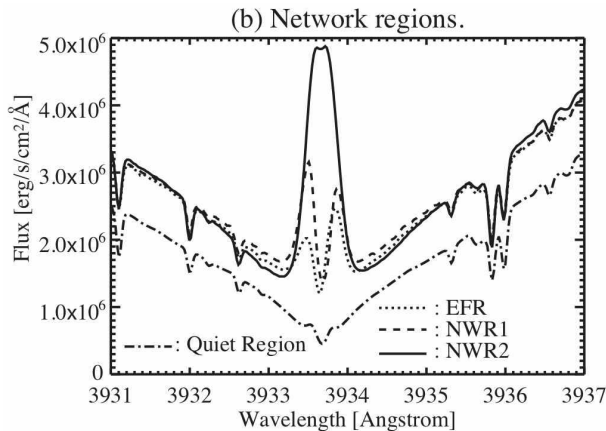


Fig. 3. Time series of the SOT BFI Ca II H intensity curve (solid line) at the locations on the same polarity inversion line where the "Jet09-0031" occurred: This intensity curve was made as tracking the locations of the same polarity inversion line, which was moving (cf. Fig. 6). Sampled area is 1."09 ϕ (~800km ϕ) disk, and the intensities are averaged in it (in arbitrary unit). The first large peak represents the "Jet09-0031", and the strongest peak around 00:45 UT represents the "Jet09-0045" (see the peaks indicated by oblique hatching). Each square with a number on this curve corresponds to the timing of a row in Fig. 6 and of a Ca II K spectra in Fig. 7, with the corresponding number, respectively. The horizontal black bars near the top of this figure show the DST/VS data coverage.

noticed that this intensity increase around K_1 is possibly due to the presence of jet. The spectra from the nearest Ca II network regions show similar intensity variation with spectra of the Ca II network regions in the field of view, and larger than that of the quiet region (Fig. 5b). The difference in the K_3 core of the network regions' spectra, as shown in Fig. 5b, comes due to the existence of dark filament above the jet region (see Fig. 4c and $H\alpha$ images in Fig. 24 for more details). Fig. 5c shows the intensity of the jet subtracted by the background network intensity. This intensity distribution will be used later (in section 4) to estimate the released energy during the jet event.

Figure 6 shows snapshots of the evolutions of the region above the PIL, with enlarge the area around the jets. The jets occurred intermittently. We find that the timings and the shapes of the emission features in K_{1R} correlated well with the occurrences of the jets in the Ca II H broadband filter images. The K_{2R} counterpart of the jet was seen only during onset of "Jet09-0031". No K₃ counterpart were seen in any frame, while a K₃ filament was seen covering the jet region with the same alignment of the array of the photospheric magnetic sources that are involved in the series of the jet events. It is found that all the jets occurred along the same polarity inversion line. The occurrence of the "magnetic flux cancellation" around the polarity inversion line is suggestive of shrinking of the isolated negative polarity. This is confirmed by the curves of the total magnetic flux and the area size of the negative





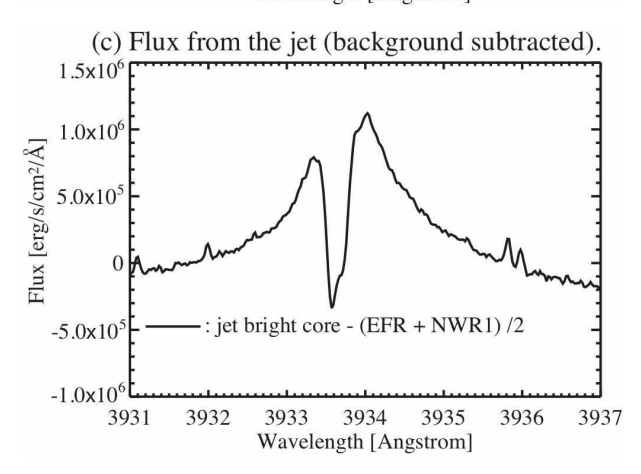


Fig. 5. Ca II K spectra of the "Jet09-0031" at 00:27:45UT of (a) jet bright core at the center of the cross-hairs in Fig. 4 (solid curve), an EFR and a network region near by this jet (EFR and NWR1; dotted and broken curves), and quiet region outside of the moat region (dash-dotted curve), (b) EFR and network regions at two locations (EFR, NWR1, and NWR2) indicated in Fig. 4, and (c) subtracted profile of ("jet bright core" — "(EFR+NWR1)/2"): The vertical axis shows the flux emitted at the solar surface. Each spectrum is made with averaging the spectra in a sample region.

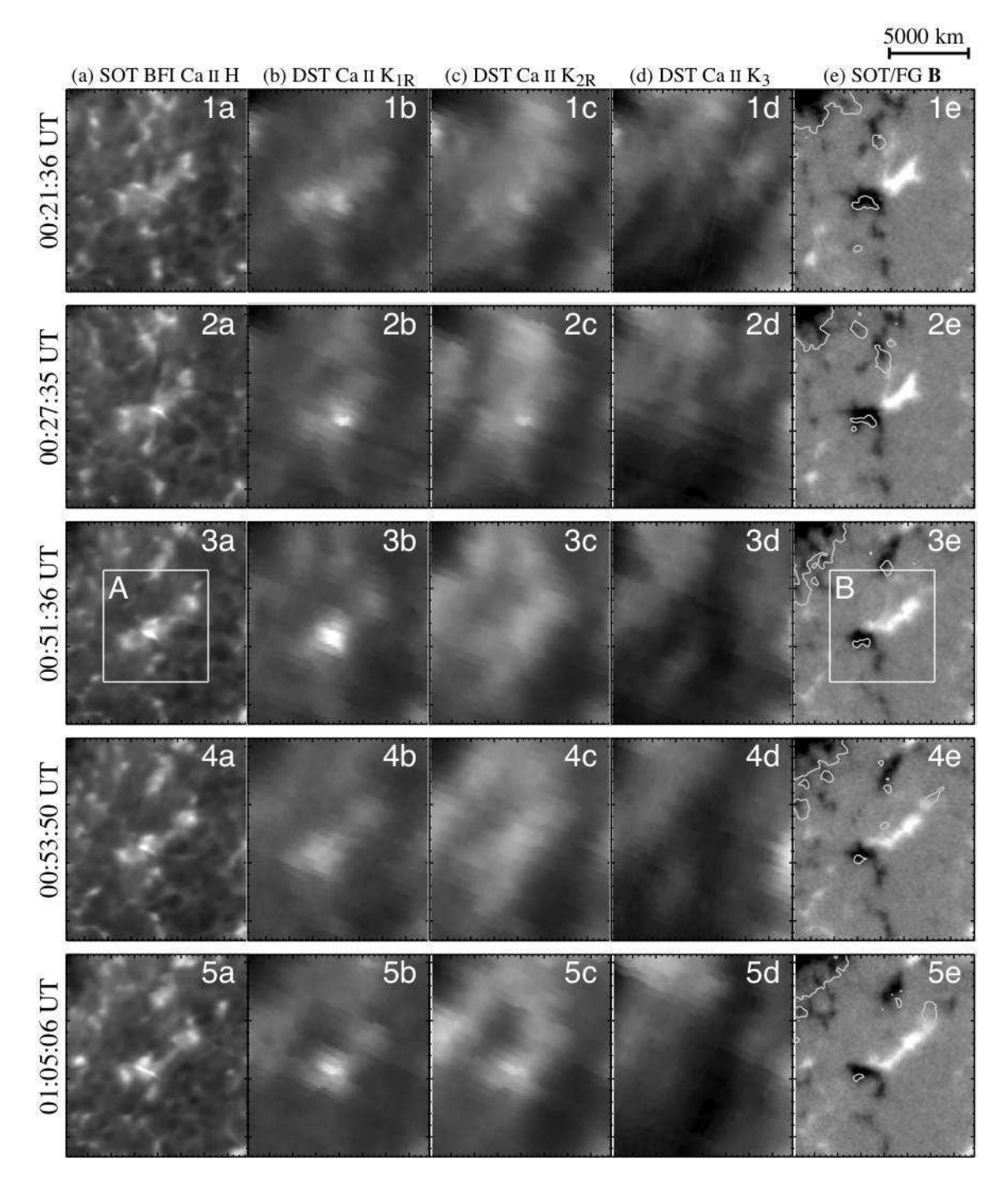


Fig. 6. Evolutions of a series of chromospheric jet events on August 9 around 00:45 UT: (a) SOT Ca II H BFI images. DST/Hida spectroheliograms of (b) Ca II K_{1R} , (c) Ca II K_{2R} , and (d) Ca II K_3 . (e) SOT NFI Fe I 6302 Å magnetograms. The time of rows are chosen as correspond to the squares with the same numbering in Fig. 3. Top is north and left is east. Each image has the same FOV of $15.''6\times14.''4$. In frames (e), white and black colors represent positive and negative line-of-sight component of the photospheric magnetic field **B** (color is saturated at ± 300 Gauss), while the contours show the horizontal components of **B** (contour level: 200 Gauss). The smaller FOVs "A" and "B" in the 3rd row represent the FOV of Fig. 27. In this figure, three chromospheric jets occurred on the same polarity inversion line. The 2nd, 3rd, and 5th rows show "Jet09-0031", "Jet09-0045", and another minor jet, respectively.

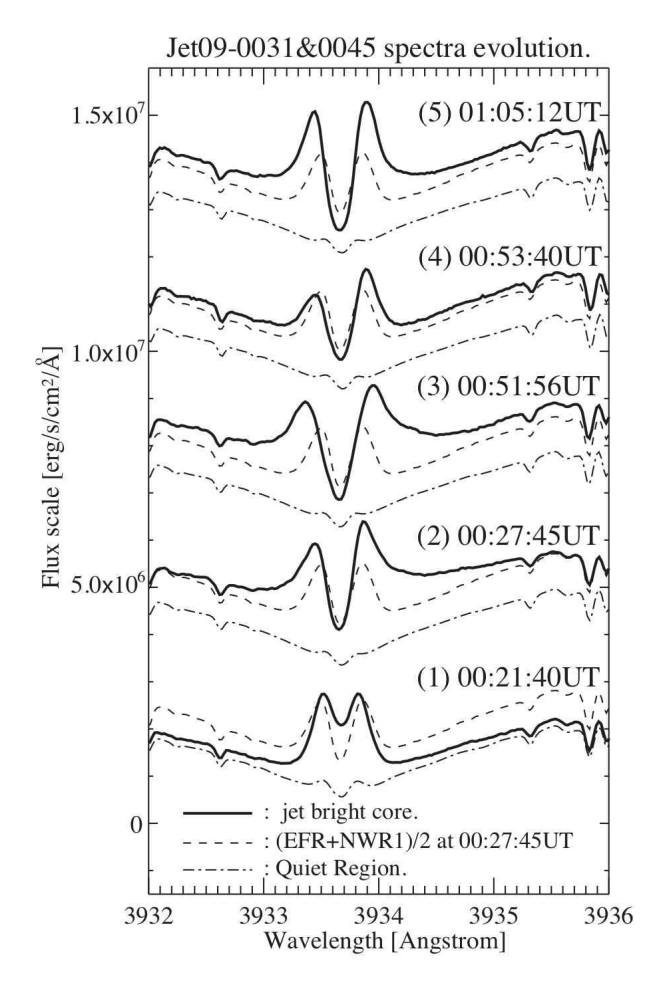
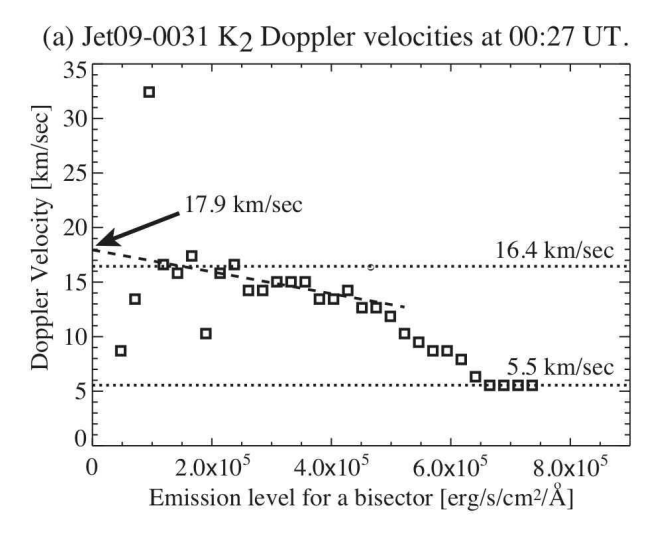


Fig. 7. Evolution of Ca II K spectra of the jets' bright cores in the series of jet events on August 9 around 00:45 UT: The time evolution in this figure is from the bottom to the top. The time of each spectrum is chosen as the same timing of a row in Fig. 6 with the corresponding number. The solid curves indicate the spectra of the jet bright cores ((2), (3), and (5)), or those of the corresponding locations but rather in quiet condition ((1) and (4)). Each spectrum is made with averaging the spectra in a sample region (0."96 ϕ (~700km ϕ) disk). Two reference spectra (of quiet region (dash-dotted curve) and of the network region near by the jet bright core at 00:27:45 UT (broken curve)) are over plotted for showing intensity increases with jets. Basically, jet bright cores in this event series are "red asymmetry" and bright at K₁.

magnetic sources shown in Figure 9. The positive polarity source that formed the polarity inversion line didn't show the "shrinkage" because this magnetic source consists of a newly emerging dipole (EFR) and new flux were supplied intermittently from the north.

Figure 7 shows time evolution of the Ca II K spectra of the jets bright cores with the same timings as mentioned in Figure 6. The jet bright cores in this series of jet events show "red asymmetries" and were bright around K_1 . Since the spectral range of the emission increases up to + 1.2 Å (in red wing) from the Ca II K line center, we interpreted that this "red asymmetries" are not the apparent shape by the blue shift of the K_3 absorption line but the actual red shift of the K_2 emission itself. We also estimated the



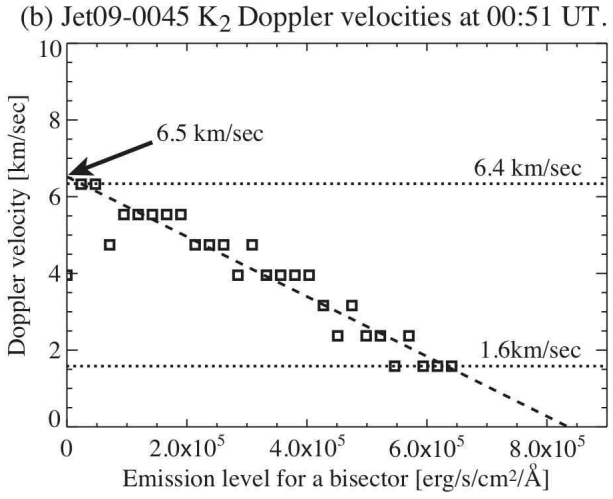


Fig. 8. K_2 Doppler velocities for (a) "Jet09-0031" and (b) "Jet09-0045": These Doppler velocities are estimated by measuring the bisector positions of the two flanks of the emission profile in K_1/K_2 . Averaged back ground spectra from near jet location was subtracted beforehand (cf. Fig. 5c). Velocities are measured at different intensity levels of an emission curve and plotted in these figures. Lower intensity level for the bisector reflects lower atmosphere.

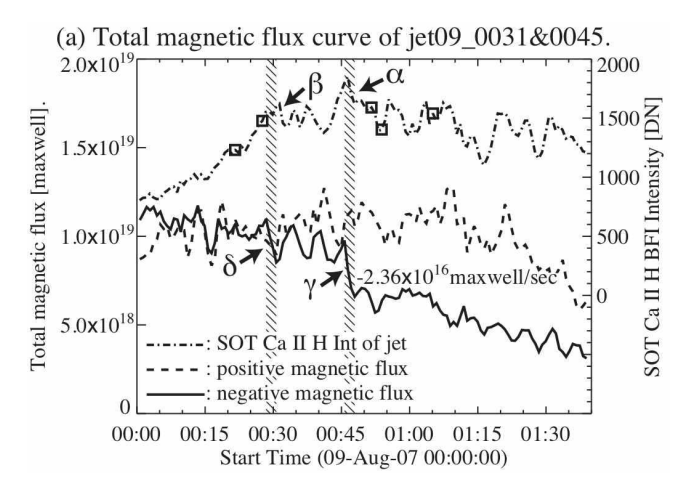
Doppler velocity of the red "asymmetries" (Fig. 8a, 8b). The Doppler velocities (Fig. 8a and 8b) are estimated by measuring the bisector positions of the profiles outside the $\rm K_2$ emission peaks. The averaged back ground spectra near the jets location were subtracted before carrying out the velocities measurements (cf. Fig. 5c). Velocities are measured at different intensity levels of an emission curve and plotted. Lower intensity level corresponds to the lower atmosphere. The estimated Doppler velocities of the emission increase in $\rm K_2/K_1$ component are approximately 5.5 km/s – 16.4 km/s (red shifted) for an onset of "Jet09-0031" and are approximately 1.6 km/s – 6.4 km/s (red shifted) for a decay phase of "Jet09-0045". In any case, larger Doppler velocities are found in lower intensity levels for making the bisector (Fig. 8a, 8b).

Figure 9 shows evolutions of the total magnetic flux and the area of the magnetic sources forming the polarity inversion line at the footpoints of the jets. A distinct magnetic flux cancellation of the negative polarity source is seen at the same time with the jet occurrence ("Jet09-0045"). We confirmed that this distinct flux cancellation actually occurred just below this jet (Appendix 2.). The measured magnetic flux cancellation rate and the decreasing rate of the negative magnetic source area associated with jets are 2.36×10^{16} Mx/s and 1.17×10^{14} cm^2/s for "Jet09-0045", respectively. For "Jet09-0031", it is 1.81×10^{16} Mx/s and 8.25×10^{13} cm²/s, respectively. Magnetic flux cancellations at the footpoints of the jets are found to occur intermittently with the jet events in the chromosphere (Fig. 9a, 9b). The jet activity in this region ceased when all the magnetic flux in negative polarity source were canceled.

Figure 10 shows an evolution of average magnetic flux density of the same magnetic sources mentioned in Fig. 9. A concentration of the negative magnetic flux is seen during the onset of "Jet09-0045". After the jet occurred, the average magnetic flux density decreased as the Ca II H intensity decreases. The similar coincidences are fairly seen for other Ca II H intensity peaks.

3.2.2. Jets associated with emerging flux (Aug. 8 0333) In this section we discuss a single jet event that occurred just near an emerging flux region. Figure 11 shows a SOT Ca II H light curve for "Jet08-0333" (see Table 1). The strong peak at the end of this light curve corresponds to this jet. The size of the jet bright core and the maximum length of this jet in SOT Ca II H images are 2–3 times larger and longer than the jets in section 3.2.1. (see Table 1).

Figure 12 shows the evolution of "Jet08-0333" with the SOT BFI and NFI and the DST/Hida spectroheliograms. The onset, peak, and decay phase of "Jet08-0333" is shown. A jet having a bright cusp toward the south is clearly seen in frame (4a) (shown black arrow). This jet appeared near the positive magnetic source of an emerging dipole " α " in frame (1e) but initiated by the extension of another larger emerging dipole " β " in frame (2e). Another bright cusp in frame (2a) (shown white arrow) shows the jet "Jet08-0319" (see Table 1). This jet



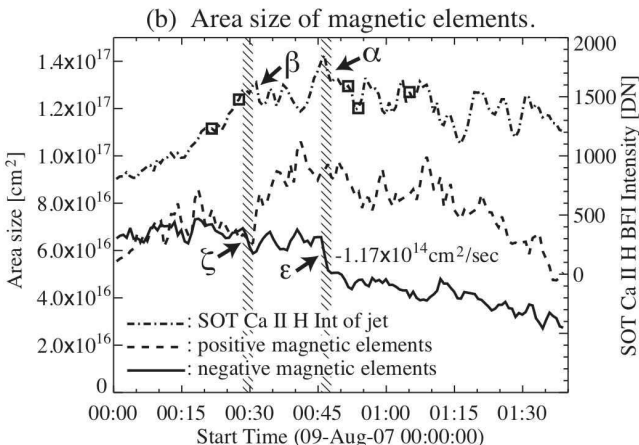


Fig. 9. Evolutions of (a) total magnetic flux and (b) area size of the magnetic sources that involved to the series of jet events on August 9 around 00:45 UT: The solid curves and the broken curves represent the plots for the isolated negative and positive magnetic sources in Fig. 27, respectively. Samplings are made by using the line-of-sight component of the photospheric magnetic field with SOT/FG magnetograms. Cut-off intensity for samplings is 42 Gauss in absolute value. The Call intensity curve from Fig. 3 is plotted as a reference of the timings of the jets (dash-dotted curves). A distinct magnetic flux cancellation (slopes γ and ϵ on the curves for the negative polarity) is seen at the same timing of "Jet09-0045" (peak α on the Ca II H light curves). Another coincidence is also seen with "Jet09-0031" (see β , δ , and ζ). The oblique hatching indicates the timings of those magnetic flux cancellations.

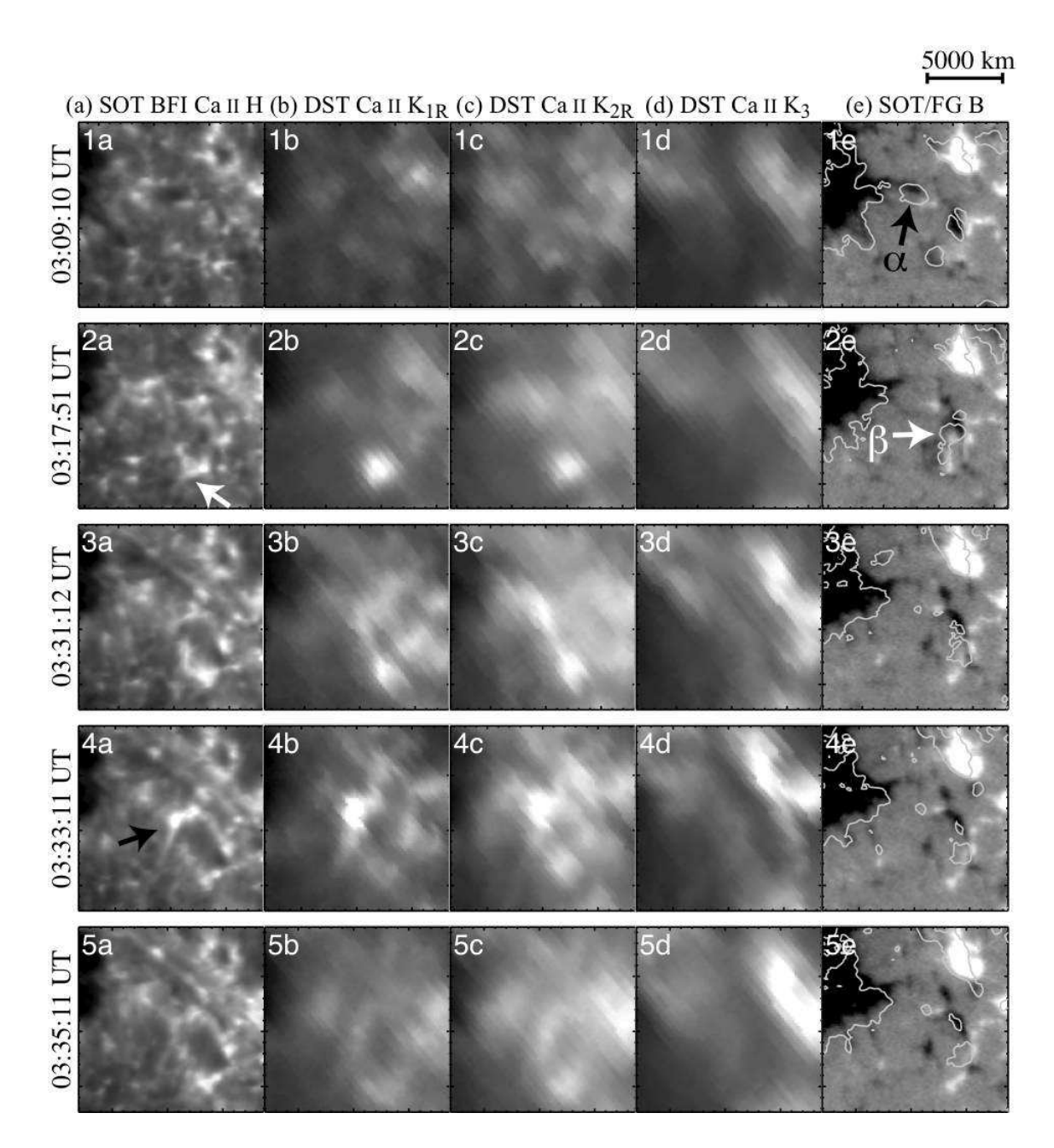


Fig. 12. Evolution of "Jet08-0333" with DST/Hida Ca II K spectroheliograms and SOT/Hinode images: Details are the same as in Fig. 6 but for "Jet08-0333". Each image has the same FOV of $16."8 \times 16."8$. Each row in this figure corresponds to a square in Fig. 11 and a Ca II K spectra in Fig. 13, with the corresponding number. The 3rd, 4th, and 5th rows represent the onset, peak, and decay phase of "Jet08-0333", respectively. A jet of the bottom direction having a bright cusp at its footpoint is clearly seen in frame (4a) (shown black arrow). This jet appeared above the positive magnetic source of an emerging dipole magnetic source " α " in frame (1e) but initiated by the extension of another larger emerging dipole " β " in frame (2e). The bright cusp in frame (2a) (shown white arrow) is the footpoint of another chromospheric jet "Jet08-0319" (see Table 1). This jet occurred at the other end of the emerging dipole " β ", and traveled to the bottom direction, same as "Jet08-0333".

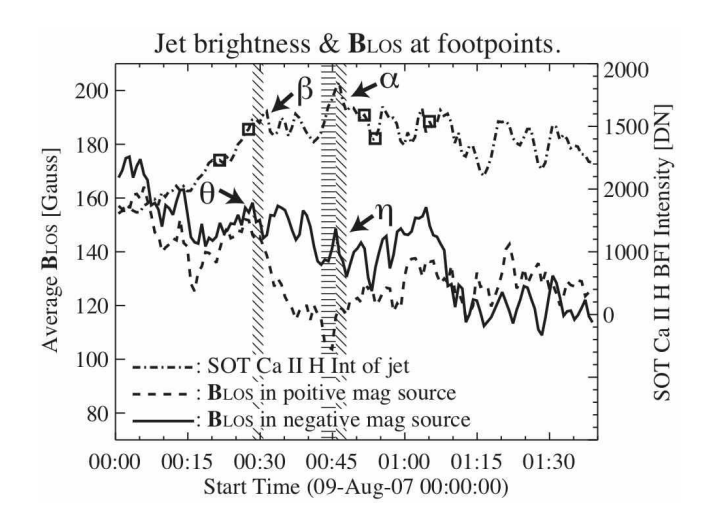


Fig. 10. The same as Fig. 9 but for average magnetic intensities of the magnetic sources that involved to the series of jet events on August 9 around 00:45 UT: A concentration of the negative magnetic flux is seen in the onset phase of "Jet09-0045" (compare the peaks α and η in horizontal hatching). After the jet occurred, the average magnetic intensity of the negative magnetic flux decreases with the CaII H intensity decrease (compare α and η in oblique hatching). The similar coincidences are fairly seen for other peaks (e.g. the peaks β and θ).

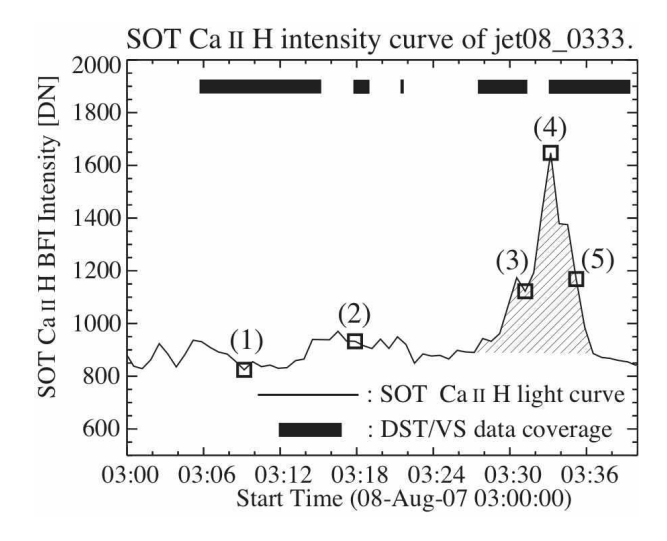


Fig. 11. Time variation of the SOT CaII H intensity (solid curve) at the location where "Jet08-0333" bright core appeared: The strong peak (oblique hatching) corresponds to "Jet08-0333" (see Table 1). Sampled area is 1."09 ϕ (\sim 800km ϕ) disk, and the intensities are averaged in it (in arbitrary unit). Tracking for the differential rotation of the sun is applied. Each square with a number on this curve corresponds to the timing of a row in Fig. 12 and of a CaII K spectrum in Fig. 13, with the corresponding number, respectively. The horizontal black bars near the top of this figure show the DST/VS data coverage.

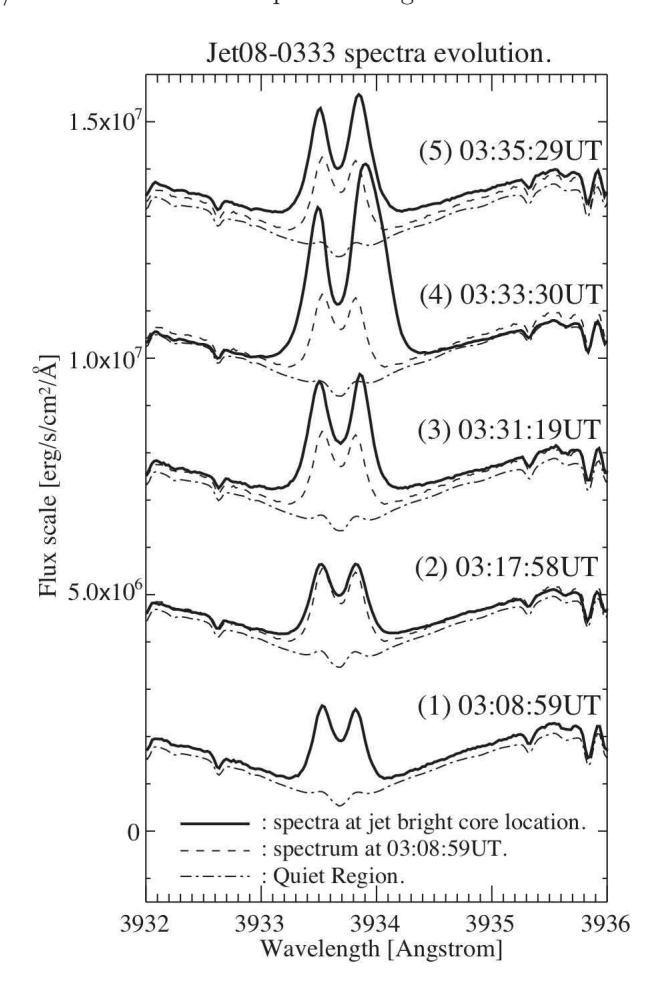


Fig. 13. Evolution of the CaII K spectra of the jet bright core of "Jet08-0333": Details are the same as Fig. 7 but for "Jet08-0333". The solid curves indicate the spectra of the jet bright core ((3): jet onset, (4): peak, and (5): decay phase), or those of the same location but rather in quiet condition ((1) and (2)). A reference spectrum (broken curves; the spectrum from 03:08:59 UT at the same location) is over plotted for showing intensity increase with the jet. This "Jet08-0333" is bright at K_1 , same as the jets "Jet09-0031" and "Jet09-0045" in Fig. 7. The "red asymmetry" is obvious only at the peak phase.

occurred at the other end of the emerging dipole " β ", and was ejected into a southward direction, same as "Jet08-0333". In any case, the jets or jet bright cores are bright at K_1 and K_2 . The K_1 images show better contrast jet structures.

Figure 13 shows the time evolution of Ca II K spectra of "Jet08-0333". "Jet08-0333" is bright at K_1 , same as the jets "Jet09-0031" and "Jet09-0045" in Fig. 7. The "red asymmetry" is obvious at the peak phase. Estimated K_2 Doppler velocities for the "red asymmetry" using the bisector positions of the emission profile (cf. section 3.2.1) are approximately $2.4~\rm km/s-5.5~km/s$ red shifted. Larger Doppler velocities are found in higher emission levels for the bisector, in contrast to the jets mentioned in section 3.2.1 (Fig. 14).

Figure 15 shows evolution of total magnetic flux and

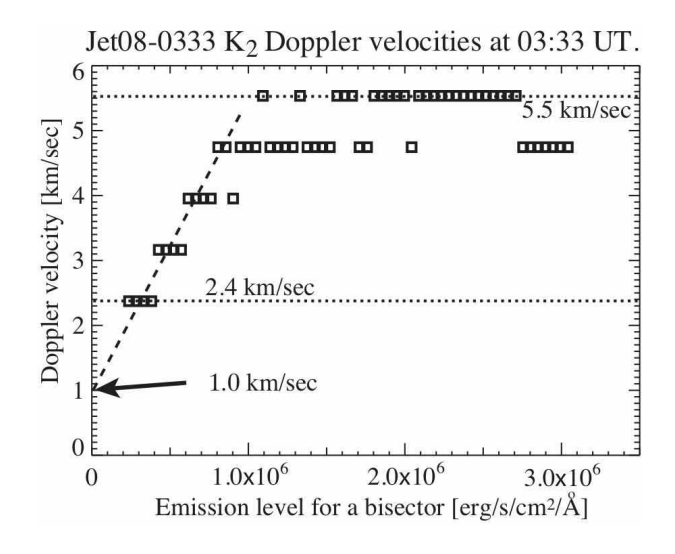


Fig. 14. K_2 Doppler velocities for "Jet08-0333": Details are the same as in Fig. 8.

area of the magnetic sources involved in the "Jet08-0333". No distinct magnetic flux cancellation is seen during the same time of the "Jet08-0333", but a cancellation of the positive magnetic flux of an emerging dipole " α " (see Fig. 12(1e)) is seen about 8 minutes before the CaII H jet.

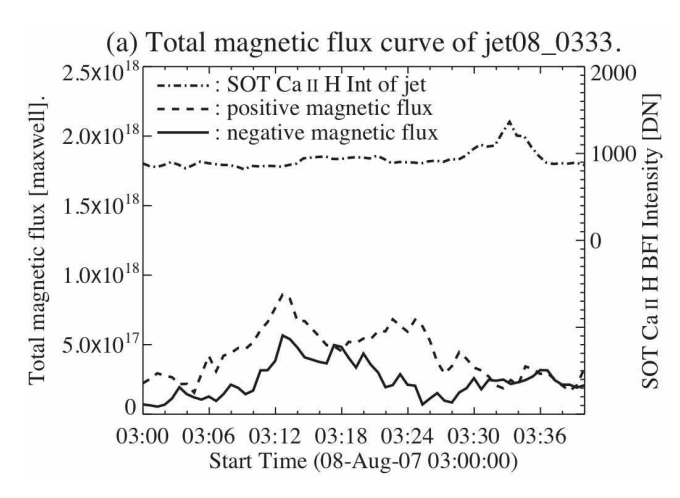
3.2.3. Jets associate with MMFs (Aug. 8 0046)

In the previous sections 3.2.1 and 3.2.2, chromospheric anemone jets occurred on a polarity inversion line that is involved in one or two emerging fluxes (EFR). In this section we introduce a different case, i.e. a chromospheric anemone jet on a polarity inversion line formed between a moving magnetic feature (MMF) and satellite magnetic patches of opposite polarity.

Figure 16 shows time variation of the SOT Ca II H intensities by tracking the locations of an MMF where "Jet08-0046" bright core appeared. The strong peak around 00:40 UT corresponds to the "Jet08-0046" (see Table 1). The life time of the "bright core" of this jet is around 320 seconds, but the jet itself seems to have shorter life time (cf. Table 1 for more details).

Figure 17 shows the evolution of "Jet08-0046" with the SOT BFI and NFI and the DST/Hida spectroheliograms. In this figure, blue wing images, K_{1V} and K_{2V} , are chosen instead of the red wing that is chosen in previous figures since it is brighter in the blue wing of the Ca II K line. A jet of the leftward direction is fairly seen in frame (4a) (see white arrow for the jet bright core). This jet occurred above a southward traveling MMF, which had left the south edge of the sunspot. This MMF seemingly collided with other magnetic elements, and then the jet occurred.

Figure 18 shows time evolution of the Ca II K spectra of the jet. In contrast to the spectra of the jets with emerging dipole magnetic sources ("Jet08-0333", "Jet09-0031", and "Jet09-0045"), "Jet08-0046" shows "blue asymmetry". Estimated K_2 blue shifted Doppler velocities for the "blue asymmetry" are approximately 1.6 km/s - 4.7



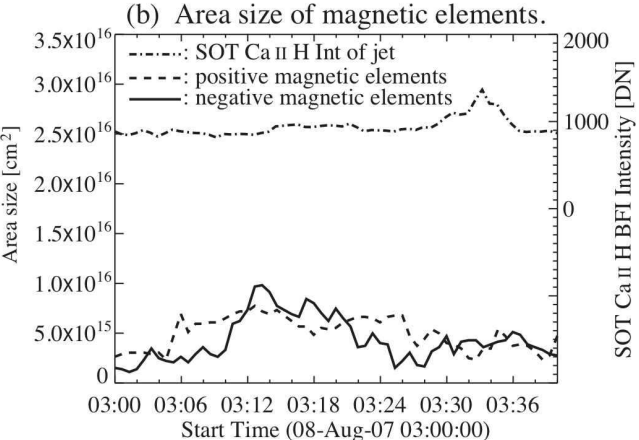


Fig. 15. Evolutions of (a) total magnetic flux and (b) area size of the magnetic sources that involved to "Jet08-0333": Details are the same as in Fig. 9 but for "Jet08-0333". Samplings are made for the area of 3."84 ϕ (\sim 2800km ϕ) disk, centered at the location of the jet bright core. Tracking for the differential rotation of the sun is applied. No distinct magnetic flux cancellation is seen at the same timing of the "Jet08-0333", but a cancellation of the positive magnetic flux is seen about 8 minutes before the jet peak.

km/s. Larger Doppler velocities are found in the lower emission levels for the bisector, same as the jets mentioned in section 3.2.1 (see Fig. 19).

Figure 20 shows evolutions of total magnetic flux and area of the magnetic sources that is involved in the "Jet08-0046". Samplings are made for the area of 6."4 ϕ (~4700km ϕ) disk, centered at the locations of the MMF with tracking it. A cancellation of the negative magnetic flux is seen simultaneously with the "Jet08-0046" event. This negative magnetic flux involved in the satellite magnetic patches of negative polarity collided with the MMF (see Fig. 17).

4. Discussions

4.1. Estimates of energy release rate

In this section we estimate the energy release rate of the chromospheric jets by two different methods, (1) from the

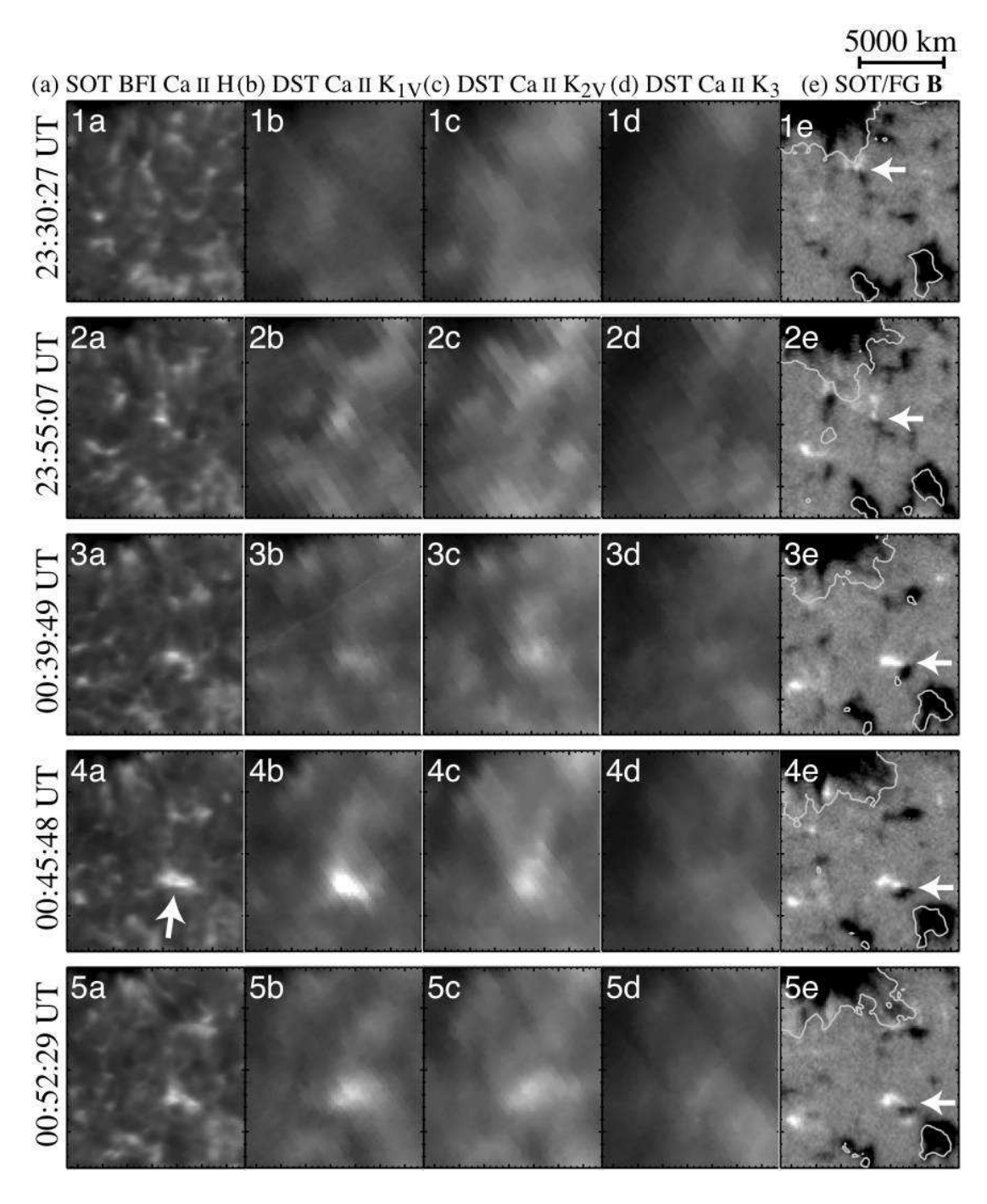


Fig. 17. Evolution of "Jet08-0046" with DST/Hida Ca II K spectroheliograms and SOT/Hinode images: Details are the same as in Fig. 6 but for "Jet08-0046", and Ca II K_{1V} and Ca II K_{2V} are chosen instead of the red wing spectroheliograms. Each image has the same FOV of 14."4×16."2. Each row in this figure corresponds to a square in Fig. 16 and a Ca II K spectra in Fig. 18, with the corresponding number. The 3rd, 4th, and 5th rows represent the onset, peak, and decay phase of "Jet08-0046", respectively. A jet of the leftward direction is seen in frame (4a) (shown white arrow). This jet appeared above a southward traveling MMF, which had left the south edge of the sunspot (shown white arrows in frames (1e)–(5e)). This MMF seemingly collided with other magnetic elements, then the jet occurred.

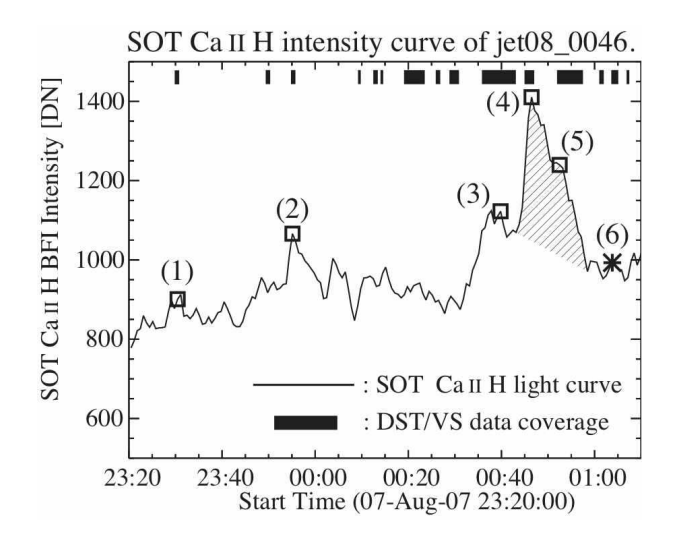


Fig. 16. Time variation of the SOT CaII H intensity at the location on a moving magnetic feature (MMF) where "Jet08-0046" bright core appeared: The strong peak (oblique hatching) corresponds to the "Jet08-0046" (see Table 1). This intensity curve was made as tracking the locations of a MMF, which was traveling (shown white arrows in column (e) in Fig. 17). Sampled area is 2."18 ϕ (~1600km ϕ) disk, and the intensities are averaged in it (in arbitrary unit). The squares with the numbers ((1)-(5)) on this curve correspond to the timings of rows in Fig. 17 and of CaII K spectra in Fig. 18, with the corresponding numbers, respectively. The asterisk, indicated by (6), represents the time of the reference CaII K spectra in Fig. 18 (broken curves). The horizontal black bars near the top of this figure show the DST/VS data coverage.

magnetic cancellation rate assuming magnetic reconnection, and (2) from the emission increase around the $\rm K_2/K_1$ on the Ca II K line profiles. By assuming two dimensional steady magnetic reconnection, the released magnetic energy can be estimated as the Poynting flux entering from both sides into the reconnecting region using the relation,

$$\frac{dE_{\text{mag}}}{dt} = 2\frac{B_{\text{ch}}^2}{4\pi} v_{\text{in}} H l_{\text{PIL}},\tag{1}$$

where $\mathrm{dE_{mag}}/dt$ is the magnetic energy release rate due to magnetic reconnection in the lower chromosphere, B_{ch} is magnetic flux density in the lower chromosphere, v_{in} is an inflow velocity to the reconnection site, $H~(\approx 150~\mathrm{km})$ is the pressure scale height in the lower chromosphere, and l_{PIL} is the length of magnetic polarity inversion line where the jet has occurred. Here we assumed that the vertical size of the reconnection region is approximately the same size as the diameter of flux tubes and that is the pressure scale height H. Since we cannot know the actual inflow velocity v_{in} in the lower chromosphere, we use a horizontal converging velocity at the photosphere as an assumption. That is given by

$$v_{\text{cancel}} = \frac{dS}{dt} l_{\text{PIL}}^{-1}, \tag{2}$$

where v_{cancel} is the horizontal converging velocity to the magnetic polarity inversion line at the photosphere, dS/dt is decreasing rate of area of the magnetic source at the footpoint of a jet. Since we have only the photospheric

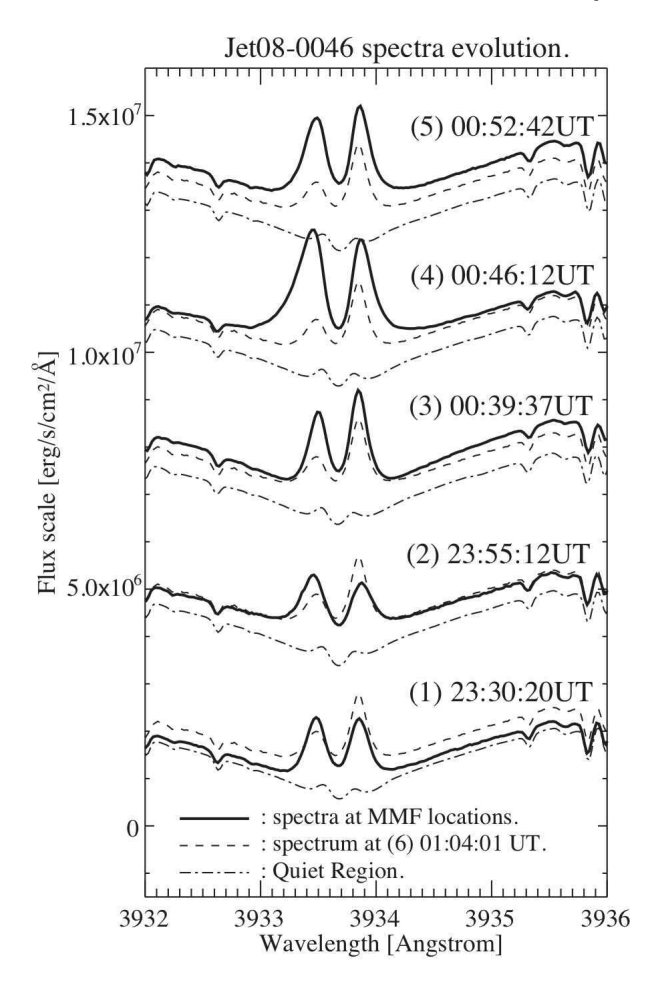


Fig. 18. Evolution of CaII K spectra of the jet bright core of "Jet08-0046": Details are the same as in Fig. 7 but for "Jet08-0046". The solid curves indicate the spectra of the jet bright core ((3): jet onset, (4): peak, and (5): decay phase), or those of the locations on the MMF with tracking but rather in quiet condition ((1) and (2)). A reference spectrum (broken curves; the spectrum from 01:04:01 UT at the MMF's location) is over plotted for showing intensity increases with jets. This reference spectrum is chosen since the MMF was traveling before the jet occurred. In contrast to the spectra of the jets with emerging dipole magnetic sources ("Jet08-0333", "Jet09-0031", and "Jet09-0045"), "Jet08-0046" is bright mainly at K_{1V} , and "blue asymmetry".

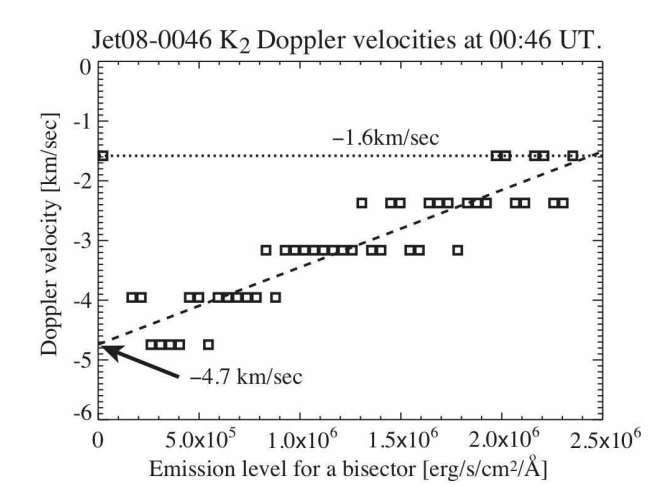


Fig. 19. K_2 Doppler velocities for "Jet08-0046": Details are the same as in Fig. 8. This event shows blue shift in K_2 component.

magnetic field observation, we estimate the chromospheric value from the following relation,

$$\frac{B_{\rm ch}}{B_{\rm ph}} = e^{-\frac{Z}{2H}},\tag{3}$$

where $B_{\rm ph}$ is a magnetic flux density in the photosphere, and Z is height of the reconnection site from the photosphere. We use the following relation for $B_{\rm ph}$ as,

$$B_{\rm ph} = \frac{d\Phi_{\rm ph}}{dt} \left(\frac{dS}{dt}\right)^{-1},\tag{4}$$

where $d\Phi_{\rm ph}/dt$ is an observed magnetic flux cancellation rate. Here $B_{\rm ph}$ is the spatially averaged value of the observed magnetic cancellation rate. We consider the "filling factor" f,

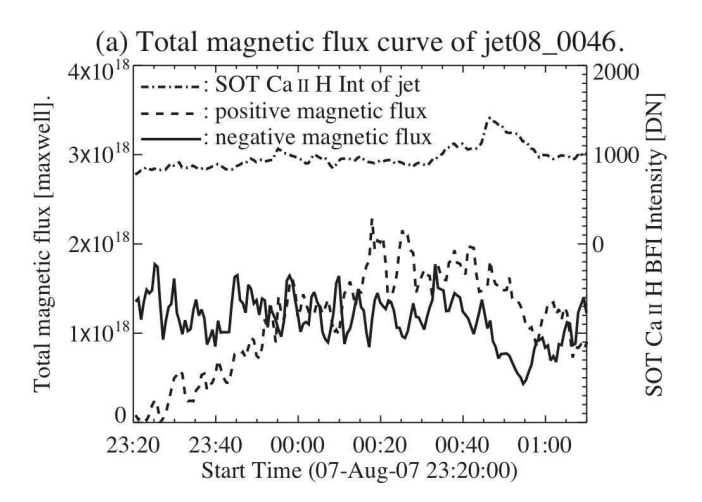
$$\overline{B_{\rm ph}} = f B_{\rm ph},\tag{5}$$

$$S = f \overline{S}, \tag{6}$$

where $\overline{B_{\rm ph}}$ and \overline{S} are observed, and $B_{\rm ph}$ and S are intrinsic magnetic flux density and area, respectively. The observed magnetic flux is $\Phi_{\rm ph} = B_{\rm ph} S = \overline{B_{\rm ph}} \overline{S}$. It is not affected by the filling factor. Finally, we get the equation for magnetic energy release rate due to magnetic reconnection in the lower chromosphere as,

$$\frac{dE_{\text{mag}}}{dt} = 2\frac{He^{-\frac{Z}{H}}}{4\pi f} \left(\frac{d\Phi_{\text{ph}}}{dt}\right)^2 \left(\frac{d\overline{S}}{dt}\right)^{-1}.$$
 (7)

Now we apply the formula to estimate the energy release rate of two jets, i.e. "Jet09-0045" and "Jet09-0031". We use f=0.15, assuming that the actual magnetic flux density of each magnetic element $B_{\rm ph}\approx 1000$ Gauss, for the observed average magnetic flux density $\overline{B}_{\rm ph}=150$ Gauss for "Jet09-0045" (η in Fig. 10). For "Jet09-0045", we have $d\Phi_{\rm ph}/dt=-2.36\times 10^{16}$ Mx/s (γ in Fig. 9), $d\overline{S}/dt=-1.17\times 10^{14}$ cm²/s (ϵ in Fig. 9), $l_{\rm PIL}=9.50\times 10^{7}$ cm, and in the lower chromosphere or upper photosphere H ≈ 150 km. Thus assuming the height of the reconnection site for the jet as $Z\approx 600$ km (lower chromosphere) or



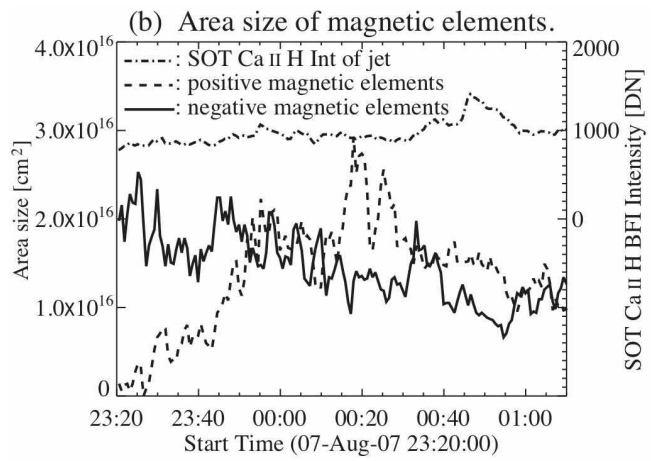


Fig. 20. Evolutions of (a) total magnetic flux and (b) area size of the magnetic sources around the locations of the MMF that involved to "Jet08-0046": Details are the same as in Fig. 9 but for "Jet08-0046". Samplings are made for the area of 6." 4 ϕ (~4700km ϕ) disk, centered at the locations of the MMF with tracking it. A cancellation of the negative magnetic flux is seen around the same timing of the "Jet08-0046". This negative magnetic flux involved in the satellite magnetic patches of negative polarity collided with the MMF (cf. Fig. 17).

 $Z \approx 300$ km (upper photosphere), we obtain from Eq. (7), $dE_{\rm mag}/dt = (1.4-10) \times 10^{24}\,{\rm erg/s}$. For "Jet09-0031", we obtain $dE_{\rm mag}/dt = (1.1-8.1) \times 10^{24}\,{\rm erg/s}$, with $d\Phi_{\rm ph}/dt = -1.81 \times 10^{16}\,$ Mx/s (δ in Fig. 9), $d\overline{S}/dt = -8.25 \times 10^{13}\,$ cm²/s (ζ in Fig. 9), and f = 0.16 (θ in Fig. 10) in the same manner.

From the integral of the emission increase around the K_2/K_1 on the Ca II K line profile (Fig. 5c) as a function of wavelength, the total flux from the the Ca II K emission for the "Jet09-0031" was 4.50×10^7 erg/s/cm². The size of the bright core of the "Jet09-0031" was 4.90×10^{15} cm² on the SOT Ca II H broadband filter images. So the estimated energy release rate of "Jet09-0031" by the Ca II K emission becomes 2.20×10^{23} erg/s. The radiative losses in the Ca II K line is about one order of magnitude lower than the total energy loss in the visible spectrum (Avrett et al. 1986, Vernazza et al. 1981). Therefore the estimated total

energy release rate of "Jet09-0031" from the emission increase will be of the order of 10^{24} erg/s. This is comparable to the magnetic energy release rate of $(1.1-8.1)\times10^{24}$ erg/s estimated by a magnetic cancellation rate.

The durations of the magnetic cancellation at the footpoint of the two jets ("Jet09-0045" and "Jet09-0031") are both 130 seconds. The estimated released magnetic energies for the jets are $(1.8-13)\times 10^{26}$ erg and $(1.4-11)\times 10^{26}$ erg, respectively. Released energy estimated by emission method gives value of the order of 10^{26} erg for "Jet09-0031" during the life time of this jet, 270 seconds.

4.2. Phenomenological model of typical chromospheric anemone jets

In this section, we discuss the origin of typical jets described in section 3 on the basis of observational data. 4.2.1. Jet09-0031 and Jet09-0045

These jets occurred around 00:31-00:45 UT on Aug. 9, 2007. The magnetic field configuration during this time is illustrated in Figure 21a. This illustration is based on the magnetogram, H α image, Ca II H image, and Ca II K spectroheliogram. The jets occur at polarity inversion line between emerging flux and pre-existing network patch. This let us to think that magnetic reconnection occurred there. Since the jets and footpoint brightening were not observed in Ca II K₃ images, the jets and reconnection must have occurred below high or middle chromosphere. How can we interpret the blueshift (2–3 km/s) of K₃? Since the jets were not seen in the K₃ images and K₃ blueshift velocity is smaller than the apparent jet velocities (5–10 km/s), the blueshift of K₃ may represent the upward motion of dark filament seen in K_3 images (Fig. 4c; see the $H\alpha$ images in Fig. 24 for the dark filament), which may be triggered by the reconnection. On the other hand, the magnetic reconnection was triggered by emerging flux, so that the reconnection point may not be in the photosphere, but around lower or middle chromosphere. So there occurs a warm downflow that is heated by reconnection in the lower chromosphere (Fig. 21b). This downflow may be the cause of the redshift of the emission increases in Ca II K_1/K_2 component at the footpoint of the jet. We note that, especially in the case of solar flares, one should be careful about the interpretation of the blue or red asymmetries of H α and Ca II K lines (e.g., Ding & Fang 1996, Ding & Fang 1997). However this time, the observed red asymmetries can be attributed to redshifts of K₂ emission since the redshifts are obtained by measuring the bisector positions of the two flanks of the K₂ emission, and the spectral range of the emission increases are wide enough comparing to the blueshifts of the K_3 absorption line. 4.2.2. Jet08-0333

This jet occurred around 03:33 UT on Aug. 8, 2007, one day before the above jets. In this case, the jet was not seen in K_3 image, while blue shift was observed in K_3 . The jet or brightening was observed in K_1 and K_2 images near the polarity inversion line between two emerging flux (Fig. 22a, 22b). Hence the reconnection may have occurred in the low or middle chromosphere, so that the

downflow may cause the redshift of the emission increases in $\text{Ca\,II}\ K_1/K_2$ component. The overall magnetic field configuration and the associated dynamics may be similar to those for Jet09-0031.

4.2.3. Jet08-0046

The environment of this jet is different from those of previous cases. In this case, the jet was triggered by moving magnetic feature (Fig. 23a, 23b). Hence the reconnection may occur in the photosphere, so that we can observe only the upward flow in lower chromosphere, which may cause the blueshift of the emission increases in Ca II $\rm K_1/\rm K_2$ component.

4.3. Relation to Other Jets and Jet-like Phenomena

In this section we compare our results with previous observations. Kubota et al. (1974) reported red asymmetry in Na D line at the root of the surges. This may be similar to red asymmetry of Ca II $\rm K_1/\rm K_2$ at the footpoint of the chromopsheric anemone jets. Such downflow may correspond to reconnection jet ejected downwards from the reconnection point.

Our observations of chromospheric anemone jets has revealed that the jets are not seen in CaII K₃ but are bright in K₁ and K₂. This is similar to the characteristics of Ellerman bombs in $H\alpha$ line (Ellerman 1917, Roy & Leparskas 1973, Kitai 1983, Qiu, et al. 2000, Geolgoulis et al. 2002, Pariat et al. 2004, Fang et al. 2006, Matsumoto et al. 2008a, 2008b, Watanabe et al. 2008). Recently, Pariat et al. (2007) observed Ellerman bombs with Ca II 8542 Å line, and found that Ca II 8542 Å line show similar "moustache" like intensity profile as in the $H\alpha$ line. So it is likely that the footpoint of the chromospheric anemone jets reported previously correspond to the Ellerman bombs. It is interesting to note that many Ellerman bombs show elongated structure (Kurokawa et al. 1982) and often become the root of surges (Roy 1973, Roy & Leparskas 1973). Geolgoulis et al. (2002) and Pariat et al. (2004) proposed the magnetic reconnection model for Ellerman bombs in which the reconnection occurs in the sea-serpent flux tubes during the resistive emergence of magnetic flux. Isobe et al. (2007) corroborated this model using 2D magnetohydrodynamic numerical simulations of emerging flux. Matsumoto et al. (2008a, 2008b) and Watanabe et al. (2008) obtained the observational support of this model using $H\alpha$ line profile analysis based on the spectroscopic observations at Hida Observatory.

If our interpretation of Ellerman bombs as the footpoint of the chromospheric anemone jets is correct, then our observations on the jets associated with emerging flux (EFR) and moving magnetic features (MMFs) give a model that is different from the previous model (Geolgoulis et al. 2002, Pariat et al. 2004, and Isobe et al. 2007). In our model, the magnetic reconnection is triggered by the collision of the EFR or the MMF with the pre-existing magnetic flux. The association of Ellerman bombs with MMFs has been observed by Nindos & Zirin (1998). The common point in these models is that the height of magnetic reconnection is low in the atmosphere, either the lower

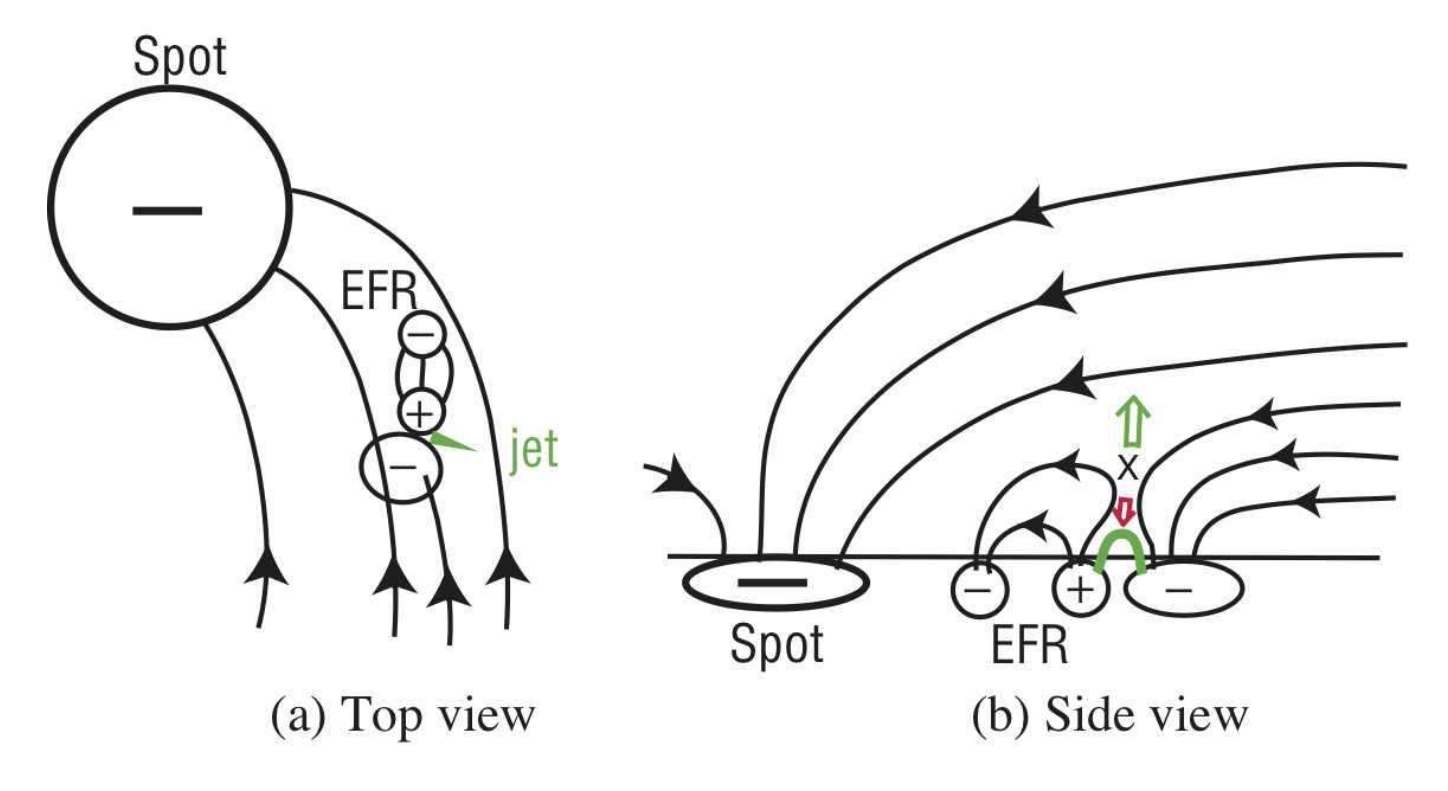


Fig. 21. A schematic diagram of "Jet09-0031" and "Jet09-0045".

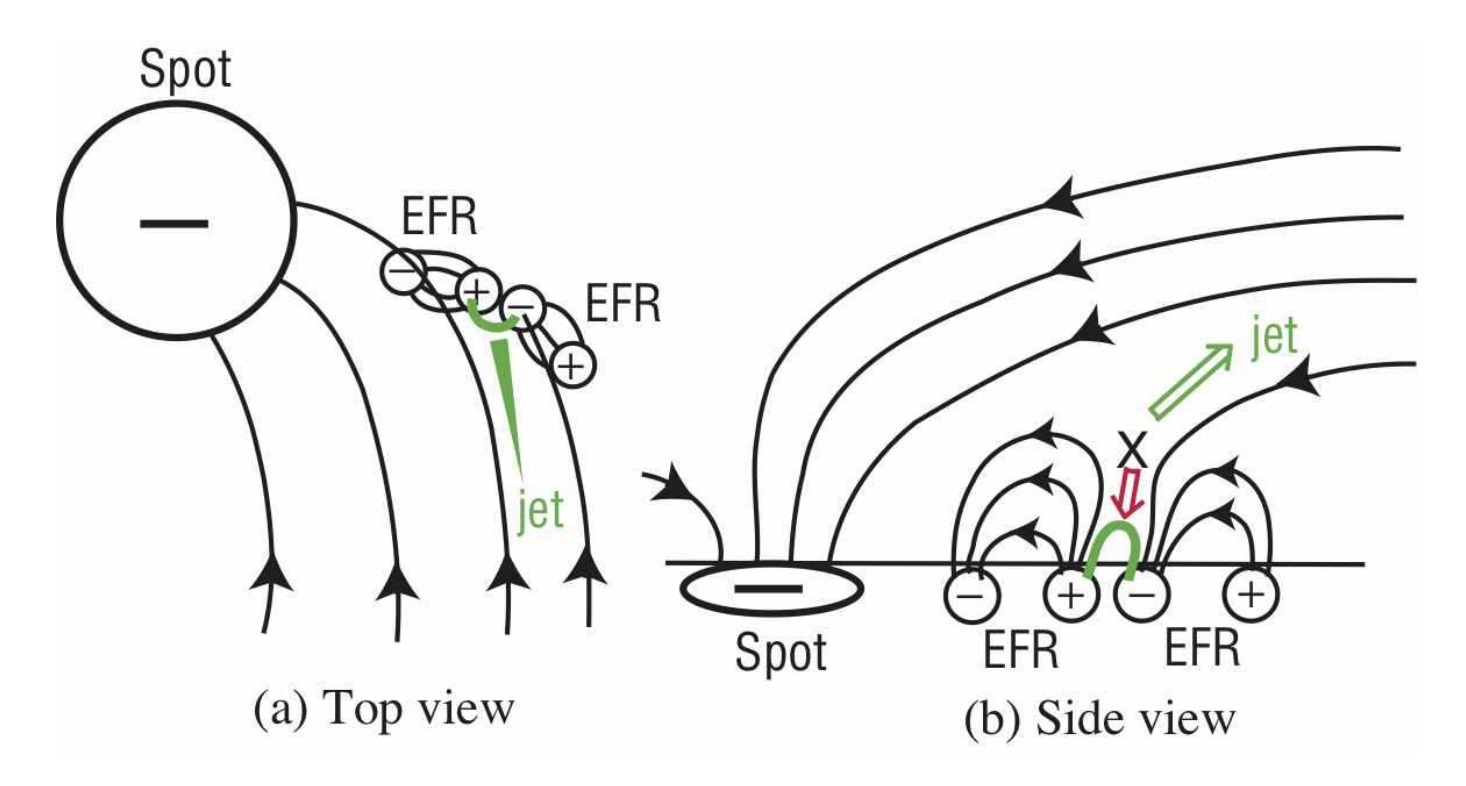


Fig. 22. A schematic diagram of "Jet08-0333".

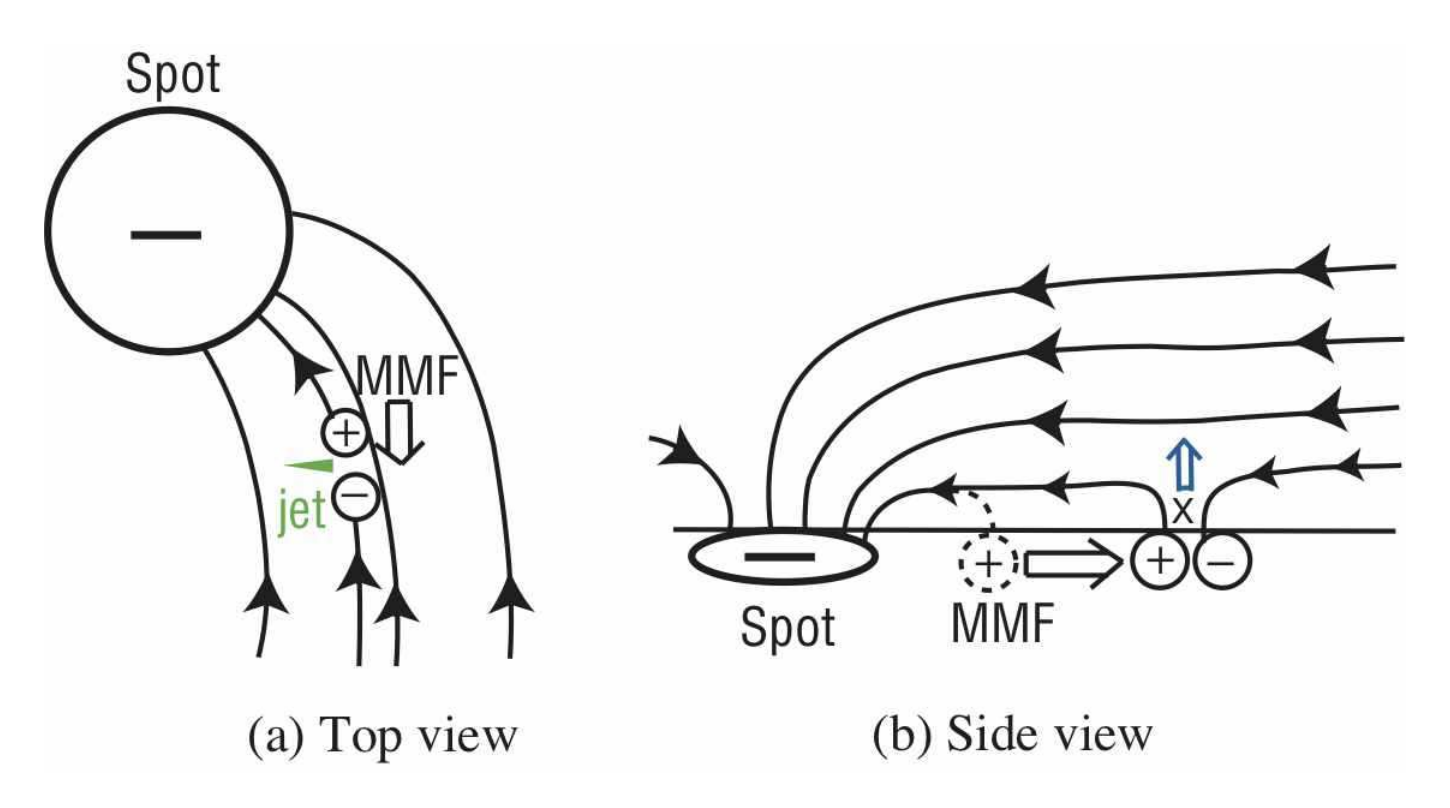


Fig. 23. A schematic diagram of "Jet08-0046".

chromosphere or the photosphere. So the numerical simulation of reconnection in the lower chromosphere and/or the photosphere (e.g., Takeuchi & Shibata 2001, Chen, Fang, & Ding 2001, Isobe et al. 2008) should be developed further.

A typical energy released in the Ellerman bombs has been estimated to be of the order 10^{26} – 10^{27} erg (Fang et al. 2006). Based on our observation, the total energy of the chromospheric anemone jets is estimated to be of the order 10^{26} erg, which is smaller than that of Ellerman bombs. This suggests that even if the basic physics of chromospheric anemone jets is similar to that of classical Ellerman bombs, the total energy and size of the chromospheric anemone jets (especially smaller ones) are smaller than those of Ellerman bombs. This collaborate the idea of Shibata et al. (2007) that there may be even smaller non-resolved reconnection events (or nanoflares) which may play an important role in heating the chromosphere and corona (Parker 1988).

Acknowledgement

This work is supported in part by the Grant-in-Aid for Creative Scientific Research "The Basic Study of Space Weather Prediction" (Head Investigator: K. Shibata) from the Ministry of Education, Culture, Sports, Science, and Technology of Japan, and in part by the Grand-in-Aid for the Global COE program "The Next Generation of Physics, Spun from Universality and Emergence" from the Ministry of Education, Culture, Sports, Science, and Technology (MEXT) of Japan. Hinode is a Japanese mission developed and launched by ISAS/JAXA, collaborat-

ing with NAOJ as a domestic partner, NASA and STFC (UK) as international partners. Scientific operation of the Hinode mission is conducted by the Hinode science team organized at ISAS/JAXA. This team mainly consists of scientists from institutes in the partner countries. Support for the post-launch operation is provided by JAXA and NAOJ (Japan), STFC (U.K.), NASA, ESA, and NSC (Norway). SM is grateful to H. Isobe for his valuable comments. SM is grateful to K.A.P. Singh and S. Yashiro for their English corrections.

Appendix 1. $H\alpha$ Observations

A.1.1. Jet09-0031 & 0045

Figure 24 shows three sets of snapshots of $H\alpha$ Lyot filter images at five wavelength positions ($H\alpha$ center and its wing at $\pm 0.5 \text{Å}$ and $\pm 0.8 \text{Å}$) for this series of jets with DST/Hida. Each image has the same field of view of Fig. 4. We use the $H\alpha$ images for examining the relation between the chromospheric anemone jets and Ellerman bombs. The corresponding locations for the jet bright cores from the SOT CaII H broadband filter images are pointed by arrows " α " in the figure.

No obvious feature is seen in the H α Lyot filter images at the five wavelength positions at the time of 8 minutes before the "Jet09-0031" Ca II H intensity peak (see 1a–1e; 4 minutes before the time of the jet onset frame (2a) in Fig. 6). Around the time of the intensity peak of "Jet09-0045" (3a–3e), the bright H α counterpart of this jet is seen in the red wing of H α (see the arrows " α " in 2d and 2e).

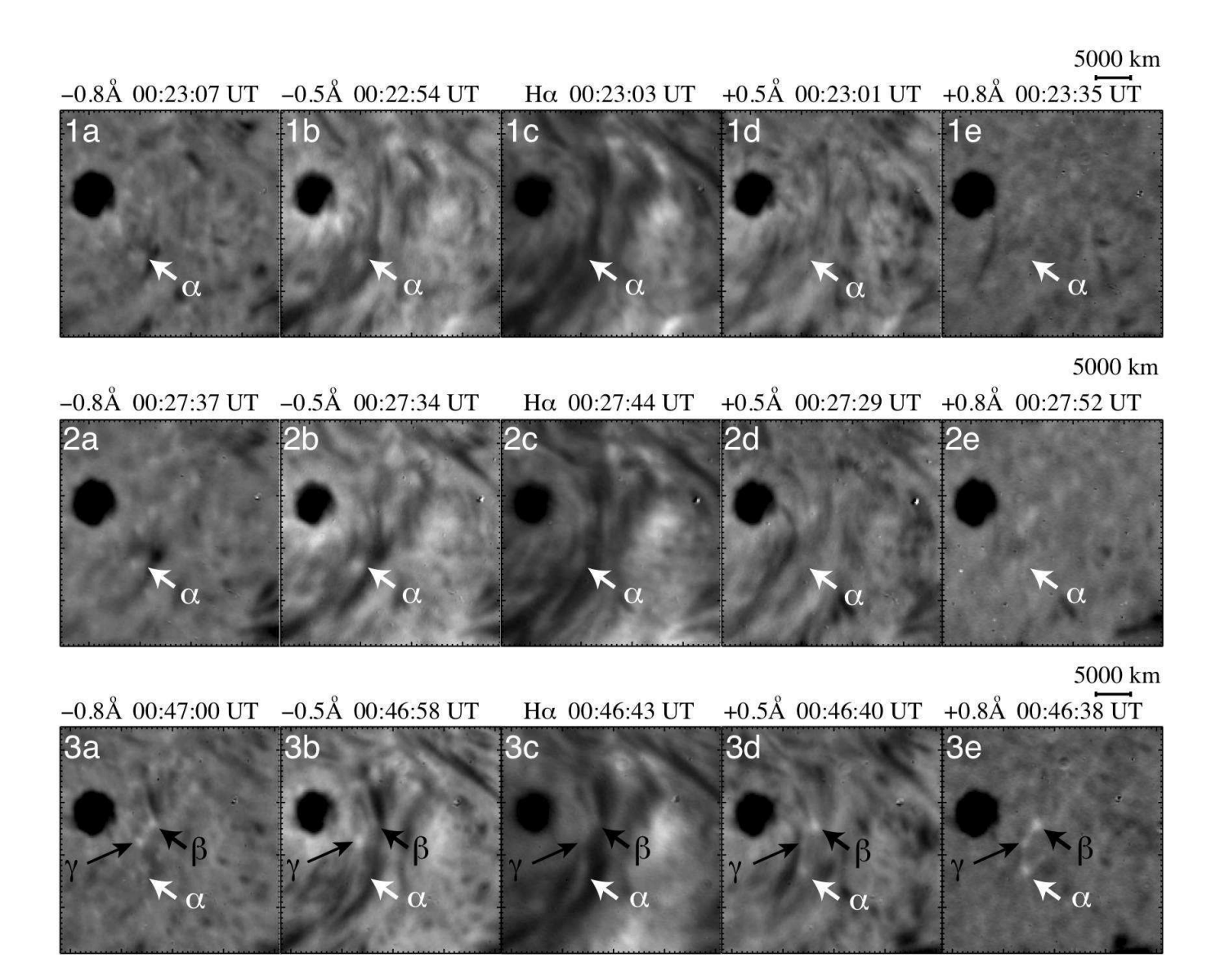


Fig. 24. Three sets of snapshots of the series of jet events on August 9 around 00:45 UT with DST/Hida H α Lyot filter images at five wavelengths positions (H α center and its wing at $\pm 0.5 \text{Å}$ and $\pm 0.8 \text{Å}$): Top is north and left is east. Each image has the same FOV of 43."2×43."2, the same FOV of Fig. 4. The white arrows " α " indicate the locations of the jet bright cores in CaII H images. The upper row (1a–1e) represents the time of 4 minutes before the 2nd row of Fig. 6 ("Jet09-0031"). No obvious feature is seen in H α at that time. The middle row (2a–2e) represents the time of the 2nd row of Fig. 6 ("Jet09-0031"). The bottom row (3a–3e) represents the time of the CaII H intensity peak of the strongest jet ("Jet09-0045") in this series of jet events (cf. 3rd row of Fig. 6). The bright H α counterpart of this jet is seen in the red wing of H α (shown arrows " α " in 2d and 2e). The locations of the other bright points " β " and " γ " correspond to another small chromospheric jets that occurred around 00:40 UT and 00:30 UT, respectively.

The locations of the other bright points " β " and " γ " correspond to another small jets that occurred around 00:40 UT and 00:30 UT, respectively. The time of the middle row (2a-2e) is chosen similar to for Fig. 4, to understand the global magnetic field orientations in the chromosphere around the jets. The orientations of the dark filaments and fibrils around the jet region were approximately from the north-northwest to the south-southeast. It is approximately in the same direction as that of the series of the centers of the magnetic elements that involved EFR.

Jet08-0333 A.1.2.

Figure 25 shows a set of snapshots of "Jet08-0333" at its SOT Ca II H intensity peak time with DST/Hida H α Lyot filter images at five wavelength positions (H α center and its wing at ± 0.5 Å and ± 0.8 Å). The white boxes represent the FOV in Fig 12. The white arrows indicate the location of the jet bright core in Ca II H broadband filter images. The bright $H\alpha$ counterpart of the jet bright core is seen in the wing of $H\alpha$, especially at -0.8Å of the $H\alpha$ line center. The black arrow in Fig. 25e indicates a surge, which appeared around the peak time of this jet, in the same location of the jet in Ca II H broadband filter images, but the length of the surge was longer. Mass motions of this surge was southward, same as "Jet08-0333". According to the shapes of fibrils and dark filaments surrounding jet region, the directions of the global magnetic field lines in the chromosphere around the "Jet08-0333" were southward.

A.1.3. Jet08-0046

Figure 26 shows set of snapshots of "Jet08-0046" at its SOT Ca II H intensity peak time with DST/Hida H α Lyot filter images at five wavelength positions (H α center and its wing at ± 0.5 Å and ± 0.8 Å). The white boxes represent the FOV in Fig 17. The white arrows indicate the location of the jet bright core in SOT Call H broadband filter images. The white arrows indicate the location of the jet bright core in Ca II H images. In this "Jet08-0046", the bright $H\alpha$ counterpart of the jet bright core is widely seen in all the five wavelength positions but faint at the $H\alpha$ line center. According to the shapes of fibrils and dark filaments in this area, the directions of the global magnetic field lines in the chromosphere around the "Jet08-0046" were in the southeast direction.

Appendix 2. Detailed evolution of a single jet "Jet09-0045"

Figure 27 shows a detailed evolution of a single jet "Jet09-0045" of the series of jets, with SOT Ca II H broadband filter images and with SOT/FG magnetograms. This time series corresponds to the strongest single peak of Ca II H intensity curve, and the same timing of that the largest magnetic flux cancellation around the polarity inversion line occurred (cf. γ in Fig. 9). The diamonds show the footpoints locations of the bright cusp of this jet at the time of the Ca II H intensity peak (frame A3). It is obvious that the footpoints of the jet ("Jet09-0045") was

the most actively colliding area between the two opposite polarity magnetic sources. The positive polarity magnetic source, which is involved in an EFR in the north, was actively entering into the isolated negative source from its northwest. Then a part of this negative source was, seemingly, "disappearing". The bright cusp of the jet appeared in this timing.

References

Alexander, D., & Fletcher, L. 1999, Sol. Phys., 190, 167 Avrett, E. H., Machado, M. E., & Kurucz, R. L. 1986, The lower atmosphere of solar flares, pp. 216-281, 216

Beckers, J. M. 1972, ARAA 10, 73

Beckers, J. M., Bridges, C. A., & Gilliam, L. B. 1976, A High Resolution Spectral Atlas of the Solar Irradiance from 380 to 700 Nanometers (Hanscom AFB: Sacramento Peak Obs.)

Brooks, D. H., Kurokawa, H., & Berger, T. E. 2007, ApJ, 656, 1197

Brueckner, G. E. & Bartoe, J.-D. F. 1983, ApJ, 272, 329

Canfield, R. C. et al. 1996, ApJ, 464, 1016

Cauzzi, G. et al. 2008, A&A, 480, 515

Chae, J, et al. 1999, ApJL, 513, L75

Chen, P. -F., Fang, C., & Ding, M. -D. .D 2001, ChJAA, 1, 176

Cirtain, et al. 2007, Science, 318, 1580

De Pontieu, B., et al. 2007, Science, 318, 1574

Ding, M. D., & Fang, C. 1996, Sol. Phys., 166, 437

Ding, M. D., & Fang, C. 1997, A&A, 318, L17

Ellerman, F., 1917, ApJ, 46, 298

Fang, C. et al. 2006, ApJ, 643, 1325

Geolgoulis, M. K., et al. 2002, ApJ, 575, 506

Ichimoto, K., et al. 2008, Sol. Phys., 249, 233

Isobe, H., Tripathi, D., & Archontis, V. 2007, ApJL, 657, L53 Isobe, H., Proctor, M. R. E., & Weiss, N. O. 2008, ApJL, 679,

Kitai, R. 1983, Sol. Phys., 87, 135

Kosugi, T., et al. 2007, Sol. Phys., 243, 3

Kubota, J., Kureizumi, T., & Koyama, S. 1974, PASJ, 26, 495 Kurokawa, H. et al. 1982, Sol. Phys., 79, 77

Landi degl'Innocenti, E., & Landolfi, M. 2004, Polarization in Spectral Lines (Dordrecht: Kluwer) ch11

Liu, Y., & Kurokawa, H. 2004, ApJ, 610, 1136

Matsumoto, T. et al. 2008a, PASJ, 60, 95

Matsumoto, T. et al. 2008b, PASJ, 60, 577

Nakai, Y., & Hattori, A. 1985, Memoirs of the Faculty of Science, Kyoto University, 36, 385

Nindos, A. & Zirin, H. 1998, Sol. Phys., 182, 381

Nishikawa, T. 1988, PASJ, 40, 613

Pariat, E. et al. 2004, ApJ, 614, 1099

Pariat, E. et al. 2007, A&A, 473, 279

Parker, E. N. 1988, ApJ, 330, 474

Qiu, J. et al. 2000, ApJ, 544, 157

Roy, J.-R., 1973, Sol. Phys., 28, 95

Roy, J.-R. & Leparskas, H. 1973, Sol. Phys., 30, 449

Rust, D. M. 1968, Proc. IAU Symp. No. 35, Structure and Development of Solar Active Regions, ed. K. O. Kiepenheuer. Dordrecht, D. Reidel., pp. 77-84

Savcheva, A., et al. 2007, PASJ, 59, S771

Schmieder, B., et al. 1995, Sol. Phys., 156, 245

Shibata, K., Nishikawa, T., Kitai, R., & Suematsu, Y. 1982, Sol. Phys., 77, 121

Fig. 25. A set of snapshots of "Jet08-0333" with DST/Hida H α Lyot filter images at five wavelengths positions (H α center and its wing at $\pm 0.5 \text{Å}$ and $\pm 0.8 \text{Å}$): Top is north and left is east. Each image has the same FOV of $16.''2 \times 19.''8$. The white boxes represent the FOV of Fig 12. The time of these images are chosen as around the time of the Ca II H intensity peak of this jet, and corresponds to the 4th row of Fig. 12. The white arrows indicate the location of the jet bright core in SOT Ca II H images. The bright H α counterpart of the jet bright core is seen in the wing of H α , especially in (e), at -0.8 Å of the H α line center. The black arrow in (e) indicates a surge, which appeared around this time and has the coincide location of the chromospheric anemone jet.

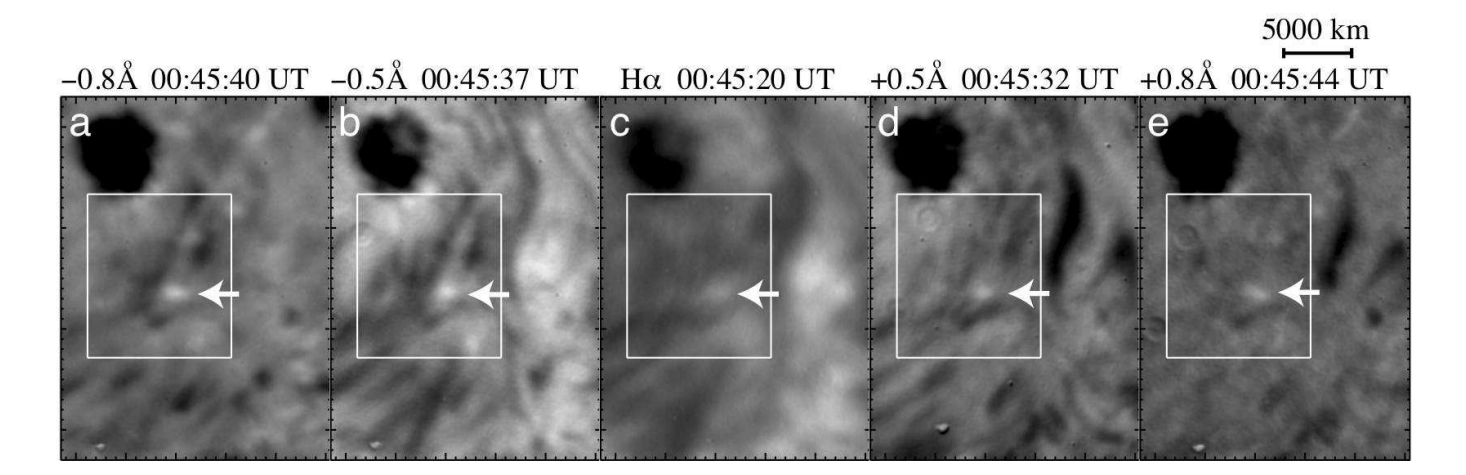


Fig. 26. A set of snapshots of "Jet08-0046" with DST/Hida H α Lyot filter images at five wavelengths positions (H α center and its wing at $\pm 0.5 \text{Å}$ and $\pm 0.8 \text{Å}$): Top is north and left is east. Each image has the same FOV of $27'' \times 36''$. The white boxes represent the FOV of Fig 17. The time of these images are chosen as around the time of the Ca II H intensity peak of this jet, and corresponds to the 4th row of Fig. 17. The white arrows indicate the location of the jet bright core in SOT Ca II H images. In this "Jet08-0046", the bright H α counterpart of the jet bright core is widely seen in the all five wavelengths positions but faint at the H α line center.

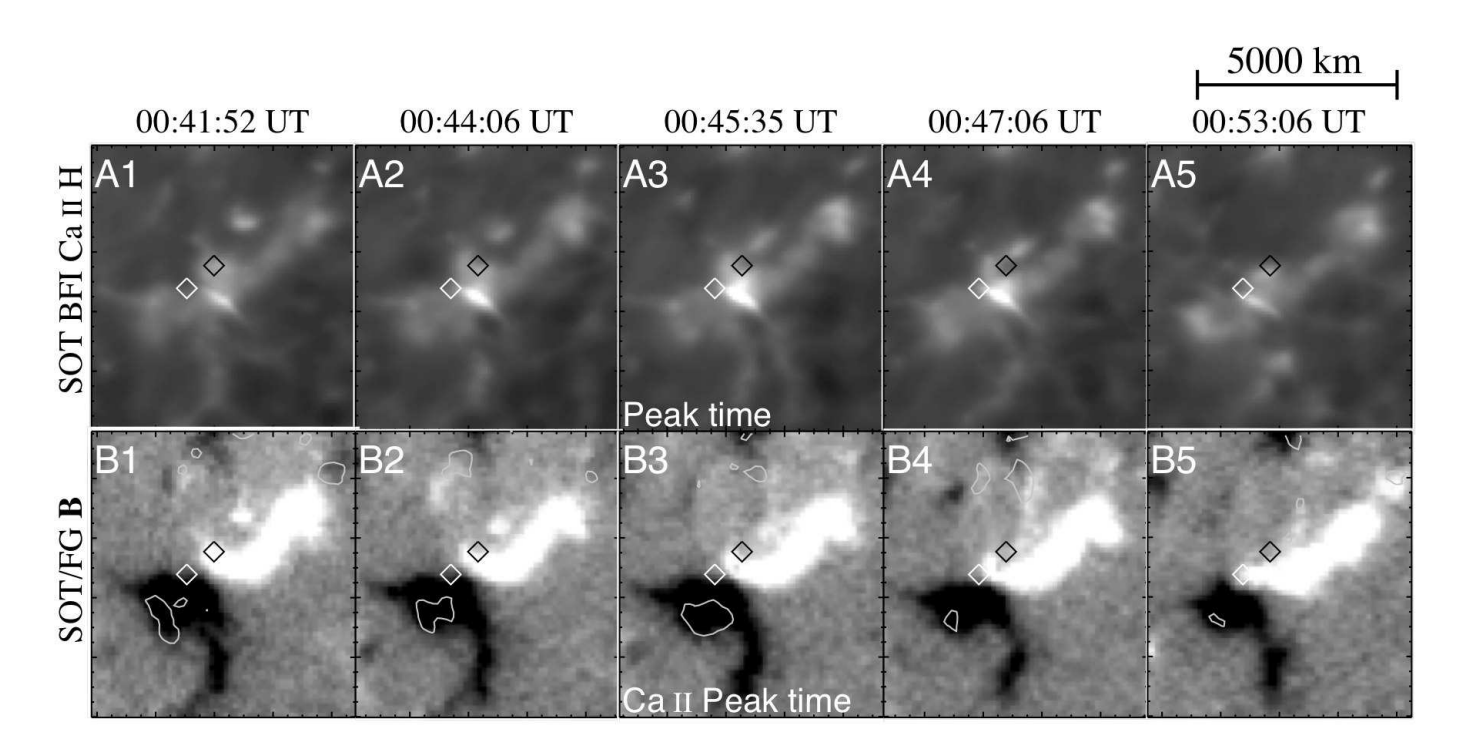


Fig. 27. Detailed evolution of a single jet "Jet09-0045", in the series of jet events shown in Fig. 6, with the SOT BFI CaII H (upper panels) and with the SOT/FG magnetograms (lower panels): Top is north and left is east. Each image has the same FOV of 9"×9."6. In the magnetograms, the white and black gray scale color shows the positive and negative line-of-sight component of the photospheric magnetic field **B** (color is saturated at ±150 Gauss), while the contours show the horizontal components of **B** (contour level: 200 Gauss). The diamonds show the footpoints locations of the bright cusp of this jet at the time of the CaII H intensity peak (see A3). This time series corresponds to the strongest single peak of the CaII H light curve, and the same timing of the largest magnetic flux cancellation (cf. Fig. 9).

Shibata, K. et al. 1994, ApJL, 431, L51
Shibata, K. 1999, Astrophys. Space Science, 264, 129
Shibata, K., et al. 2007, Science, 318, 1591
Shimojo, M. et al. 1996, PASJ, 48, 123
Shimojo, M., Shibata, K., & Harvey, K. L. 1998, Sol. Phys., 178, 379
Shimojo, M. et al. 2007, PASJ, 59, S745
Sterling, A. C. 2000, Sol. Phys., 196, 79
Suematsu, Y., Wang, H., & Zirin, H. 1995, ApJ, 450, 411
Suematsu, Y., et al. 2008a, Sol. Phys., 249, 197
Suematsu, Y., et al. 2008, in Proc. of First Results from Hinode, ASP conf series vol. 397, pp. 27-30
Takeuchi, A., & Shibata, K. 2001, ApJL, 546, L73
Tsuneta, S., et al. 2008, Sol. Phys., 249, 167
Vernazza, J. E., Avrett, E. H., & Loeser, R. 1981, ApJS, 45,

Shibata, K. et al. 1992, PASJ, 44, L173

Watanabe, H., et al. 2008, ApJ, 684, 736

Yokoyama, T. & Shibata, K. 1995, *Nature*, 375, 42 Yokoyama, T. & Shibata, K. 1996, PASJ, 48, 353